



# Multi-Mode Waveform Tomography of the Indian Ocean Upper and Mid-Mantle Around the Réunion Hotspot

M. D. Wamba, J.-P. Montagner, B Romanowicz, G Barruol

## ► To cite this version:

M. D. Wamba, J.-P. Montagner, B Romanowicz, G Barruol. Multi-Mode Waveform Tomography of the Indian Ocean Upper and Mid-Mantle Around the Réunion Hotspot. *Journal of Geophysical Research: Solid Earth*, 2021, 126 (8), pp.e2020JB021490. 10.1029/2020jb021490 . hal-03384274

**HAL Id: hal-03384274**

**<https://hal.science/hal-03384274>**

Submitted on 20 Oct 2021

**HAL** is a multi-disciplinary open access archive for the deposit and dissemination of scientific research documents, whether they are published or not. The documents may come from teaching and research institutions in France or abroad, or from public or private research centers.

L'archive ouverte pluridisciplinaire **HAL**, est destinée au dépôt et à la diffusion de documents scientifiques de niveau recherche, publiés ou non, émanant des établissements d'enseignement et de recherche français ou étrangers, des laboratoires publics ou privés.

# JGR Solid Earth

## RESEARCH ARTICLE

10.1029/2020JB021490

### Key Points:

- We performed a regional tomography of the Indian Ocean upper and mid-mantle by waveform inversion
- Two main low-velocity anomalies are found in the upper mantle beneath the western (Mascarene Basin) and the Eastern (Central Indian Basin) parts of the Ocean
- The source that feeds the hotspot volcano of La Réunion Island is anchored in the lower mantle

### Supporting Information:

Supporting Information may be found in the online version of this article.

### Correspondence to:





M. D. Wamba,  
[wamba@ipgp.fr](mailto:wamba@ipgp.fr)

### Citation:

Wamba, M. D., Montagner, J.-P., Romanowicz, B., & Barruol, G. (2021). Multi-mode waveform tomography of the Indian Ocean upper and mid-mantle around the Réunion hotspot. *Journal of Geophysical Research: Solid Earth*, 126, e2020JB021490. <https://doi.org/10.1029/2020JB021490>

Received 5 DEC 2020  
Accepted 19 JUL 2021

## Multi-Mode Waveform Tomography of the Indian Ocean Upper and Mid-Mantle Around the Réunion Hotspot

M. D. Wamba<sup>1</sup> , J.-P. Montagner<sup>1</sup> , B. Romanowicz<sup>1,2,3</sup> , and G. Barruol<sup>1</sup> 

<sup>1</sup>Université de Paris/Institut de physique du globe de Paris, UMR CNRS 7154, Paris, France, <sup>2</sup>Collège de France, Paris, France, <sup>3</sup>University of California, Berkeley, Berkeley, CA, USA

**Abstract** Réunion Island in the western Indian Ocean is well known as one of the most active volcanic hotspots on Earth. Its birth, ~65Ma ago, created the Deccan volcanic traps in India (almost 2 million km<sup>2</sup>), associated with the Cretaceous-Tertiary boundary and with the extinction of about 90% of life on the Earth, including dinosaurs. However, the deep structure of the underlying mantle, the potential presence of a rising plume and its exact geometry in the lower and in the upper mantle are still subjects of debates. The use of seismic data acquired by the French-German RHUM-RUM experiment in the Indian Ocean around the Réunion volcanic hotspot (2012–2013) and the collection of broadband seismic data from temporary experiments and from the FDSN (Federation of Digital Seismograph Networks) data center make it possible to investigate the deep structure of the Réunion mantle plume along its complete track, from its birth to its present stage, with a lateral resolution of ~600 km. So far, global seismic tomography models cannot provide such high resolution images of the transition zone or lower mantle in this region. In this study, we used the spectral element method (SEM) to perform waveform forward modeling for several thousand paths beneath the Indian Ocean, and normal mode perturbation theory to compute the gradient and the Hessian for the inverse part of the tomography. Using this hybrid method, we derived a regional tomographic model (including teleseismic and regional events) beneath the Indian Ocean, down to ~1200 km depth, from simultaneous inversion of fundamental and higher mode three components waveforms down to 40 s period. Our model retrieves a low-velocity channel extending from West to East in the western side of the Central Indian Ridge, in the depth range of 150–250 km. It also reveals a plume conduit with a broad head in the upper mantle and narrow tail anchored in the lower mantle at 1,200 km depth or deeper. The connection between the Réunion hotspot and the South-Africa Large Low-Shear Velocity Province (LLSVP) is also brought to light. Our findings suggest a long-lived Réunion hotspot, since the lower part of the conduit appears to be anchored in the lower mantle, likely fed by the African LLSVP. Our results will guide further geochemical and geodynamic studies on the interaction between the lower transition zone (660–1,000 km) and the deep lower mantle beneath the Réunion hotspot.

**Plain Language Summary** We present a model of the upper-mantle structure beneath the Indian ocean obtained by full waveform inversion of three-component seismograms collected from global and regional seismic networks, including ocean bottom stations of the RHUM-RUM project, for several thousand paths that provide good coverage of the region, with focus on the deep structure beneath the Reunion hotspot volcano. Our model features a low-velocity channel extending from West to East in the western side of the Central Indian Ridge, in the depth range of 150–250 km. It also reveals a plume conduit with a broad head in the upper mantle and narrow tail anchored in the lower mantle at 1,200 km depth or deeper, beneath the Reunion hotspot. The connection between the Réunion hotspot and the South-Africa Large Low-Shear Velocity Province (LLSVP) is also brought to light. Our findings suggest a long-lived Réunion hotspot, since the lower part of the conduit appears to be anchored in the lower mantle.

## 1. Introduction

The Indian Ocean covers a tectonically interesting area of the world, involving three principal plates (the Afro-Nubian, Antarctica and Indo-Australian plates) with some remarkable, not yet fully understood features, such as the Indian Ocean Geoid Low (IOGL), the lowest large scale geoid anomaly on earth (Negi

et al., 1987), the diffuse plate boundary between the Indian plate and the Australian continent (e.g., Bergman & Solomon, 1985; Coudurier-Curveur et al., 2020), the recent and unexpected birth of a new volcano in Mayotte in 2018 Cesca et al. (2020) or the low-velocity structure imaged in the asthenosphere beneath the Mascarene Basin (e.g., Barruol et al., 2019). Located on the African plate in the western Indian Ocean, the island of La Réunion represents the active part of a NS-trending hotspot track, which started ~65 Ma years ago with one of the most debated cataclysmic volcanic eruptions in the world, that created the Deccan Traps and changed the global climate, affecting life at that time (e.g., Courtillot et al., 1988). On Réunion Island, the active Piton de la Fournaise volcano (e.g., Five eruptions in 2019, three in 2020) is thought to represent the surface signature of a long-lasting mantle plume and the southernmost expression of this intraplate hotspot track. However, many questions remain unanswered concerning (a) the source(s) at depth that fed this powerful hotspot almost continuously since cretaceous times (e.g., Duncan, Backman & Peterson, 1990), (b) its direct or indirect anchoring at the core-mantle boundary beneath La Réunion as proposed by Morgan (1978), (c) its possible connection with the African Large Low Shear-Velocity Province (LLSVP) in the mid-mantle (e.g., Torsvik et al., 2006), (d) the presence of a vertical conduit emanating from a reservoir closer to the surface, within or above the mantle transition zone. While numerous tomographic models of large scale upper mantle seismic structure below the Indian Ocean have been produced in the last few decades (e.g., Barruol et al., 2019; Debayle & Lévêque, 1997; Lévêque et al., 1998; Mazzullo et al., 2017; Montagner, 1986; Montagner & Jobert, 1988) the seismic coverage has been greatly improved recently, owing to broadband seismic data from permanent land-based seismic stations accumulated over the last 20 years, and from a recent temporary experiment which deployed Ocean Bottom Seismometers (OBSs) in the western Indian Ocean, in the frame of the RHUM-RUM French-German experiment (e.g., Barruol & Sigloch, 2013). Many studies have been carried out over the last few years to extensively investigate upper mantle structure and anisotropy beneath and around the hotspot, using various kinds of seismic data, such as surface wave tomography (e.g., Mazzullo et al., 2017), ambient noise tomography (e.g., Hable et al., 2019), or teleseismic shear-wave splitting (Scholz et al., 2018). Lower mantle structure has also been recently investigated through body-wave tomography (Tsekhmistrenko et al., 2018). Deploying terrestrial and ocean-bottom seismic networks from the Mozambique channel to the South-West and Central Indian ridges greatly improved the data coverage and in particular allowed the construction of the first surface wave tomographic model (e.g., Mazzullo et al., 2017) with lateral resolution of ~400 km down to 300 km depth, showing the presence of a localized low-shear-velocity region beneath the Mascarene Basin, at depths between 100–200 km, called the Mascarene Basin Asthenospheric Reservoir (MBAR) (e.g., Barruol et al., 2019). The latter anomaly had already been observed by Montagner (1986) and Debayle and Ricard (2012) but with a poor resolution. From the tomographic model of Mazzullo et al. (2017), several questions were raised about its origin and its relation to the Réunion hotspot and to the neighboring ridges. However, the model resolution remained poor below 250 km depth.

The measurement of surface wave phase velocity in the Indian ocean was indeed limited to the fundamental mode, using traditional approaches to extract dispersion information from long-period seismograms (e.g., Mazzullo et al., 2017). Such a technique uses only part of the information contained in a seismogram (the phase of the fundamental mode) and does not allow to resolve structure in the transition zone and the lower mantle. Here, to better exploit the wealth of information provided by the numerous available seismograms, we apply a full waveform tomographic inversion technique using fundamental mode and overtone three-component surface waveforms. It aims at better resolving structure in the transition zone and in the upper part of the lower mantle beneath the Indian Ocean, with a focus around the Réunion hotspot. Our goal is to shed some light on the origin and shape at depth of the Réunion mantle plume and on the deep structure of the anomaly beneath the Mascarene Basin.

## 2. Tomography Data Set

Our data originate from various FDSN (Federation of Digital Seismograph Networks) permanent networks (e.g., (ASL)/USGS, 1988; Centre, 1993; GEOSCOPE, 1982; Scripps Institution of Oceanography, 1986), complemented by temporary instrumental deployments that greatly improved the data coverage beneath the SW Indian Ocean. We include data from the RHUM-RUM experiment (Barruol & Sigloch, 2011) which comprises 57 broadband Ocean Bottom Seismometers (OBSs) installed around the Réunion island and on

the neighboring ridges during the period October 2012 to December 2013, and 23 land stations temporarily deployed in La Réunion, Madagascar, and in the Iles Eparses in the Mozambique channel, during the period 2011–2015. We also used data from two companion temporary experiments in Madagascar: SELASOMA, Tilmann et al (2012), MACOMO, Wyssession et al (2011), AfricaArray Penn State University (2004), Institute Of Geophysics China Earthquake Administration (IGPCEA) (2007) and RESIF (1995). In total, we used data from ~200 regional and teleseismic events of magnitude  $5.0 \leq M_w \leq 7.0$  recorded at ~414 broad-band three-components stations. The waveforms were band-pass filtered with cut-off frequencies at 400 and 40 s and corner frequencies at 53 and 250 s. Based on group velocity windowing, the waveforms were split into wavepackets roughly separating overtone energy from fundamental mode energy as described in Li and Romanowicz (1995). Typically, a particular wavepacket contains fundamental mode energy, or overtone energy, or a mix of fundamental mode and overtone energy, depending on the distance and on the depth of the event. Furthermore, the wavepackets were weighted in order to balance the amplitudes of a given record, and to take into account the redundancy of wavepackets recorded on close-by paths. At each iteration, we computed the time-domain point-by-point misfit and the correlation between the observed and the synthetic wavepackets. To avoid cycle-skipping, at each iteration, we rejected those wavepackets for which the phase shift between data and synthetics was greater or equal to  $\pi / 2$ . This is a very conservative rejection criterion but some of the wavepackets rejected at one iteration could be admitted at the next iteration as a result of model improvement. The number of additional wavepackets at each iteration has been one indicator of the progress of the model in fitting the data as shown in supporting information (Section 5).

In Figure 2, we plot the ray coverage across the Indian Ocean showing ~1500 paths with a good azimuthal coverage, except in the southernmost part of the Indian Ocean.

The hit count maps for Rayleigh and Love waves are also plotted (Figure 3). The Rayleigh wave hit count map (Figure 3, left panel) is denser than the Love wave one (Figure 3, right panel), due to the fact that Rayleigh waves are observed on the vertical and radial components, whereas the Love wave is only recorded on the transverse component, the horizontal components being noisier than the vertical one.

### 3. Methods

Our waveform inversion uses an optimisation approach and consists in two steps at each iteration: a forward step in which the predicted seismic wavefield is computed in the current iteration model, and an inverse step in which the model is updated. For the forward modeling, we apply the spectral element method (SEM), as first developed for the spherical earth by Komatitsch and Tromp (1999) and use the code RegSEM from Cupillard et al. (2012), specifically designed for large scale regional problems in spherical geometry, providing accurate 3D synthetic seismograms without restrictions on the scale or size of heterogeneity in the model. We compute seismic waveforms, including the minor arc fundamental and higher mode surface waves, down to 40 s period, taking into account radial anisotropy. We consider the 3D global radially anisotropic shear velocity model SEMUCB-WM1 of S. French and Romanowicz (2014) as starting model for our study.

The maximum domain to propagate seismic waves allowed by RegSEM is a  $90^\circ \times 90^\circ$  chunk. In order to extend the spatial coverage and to include more teleseismic events issued from areas surrounding the Indian Ocean in our regional scale study, we use three overlapping RegSEM chunks, each of area  $90^\circ \times 90^\circ$  (Figure 1a) for the forward wavefield computations. Each chunk is a physical domain containing both sources and receivers (see red, blue and magenta domains in Figure 1a). All the sources are triggered in each physical domain allowing thousands of paths intersecting across the Indian Ocean. We ensure the non-repetition of the events between the different chunks (i.e., a source positioned within a particular chunk, cannot be found in the two other ones). The synthetic wavefield artificially reflected at the edges of the physical domain is attenuated through the implemented Perfectly Matched Layers (PML), and we keep a distance of at least half a seismic-wavelength between the physical domain that contains sources and receivers, and the border of the absorption domain (see, Festa & Vilotte, 2005). The topography of the region is taken into account and for the oceanic part we substitute the water layer by its load in the wavefield computation. The crust is replaced by an equivalent smooth and homogenized crustal model as described in supporting information (Section 2). More details on the homogenization technique of the crust can also be found in



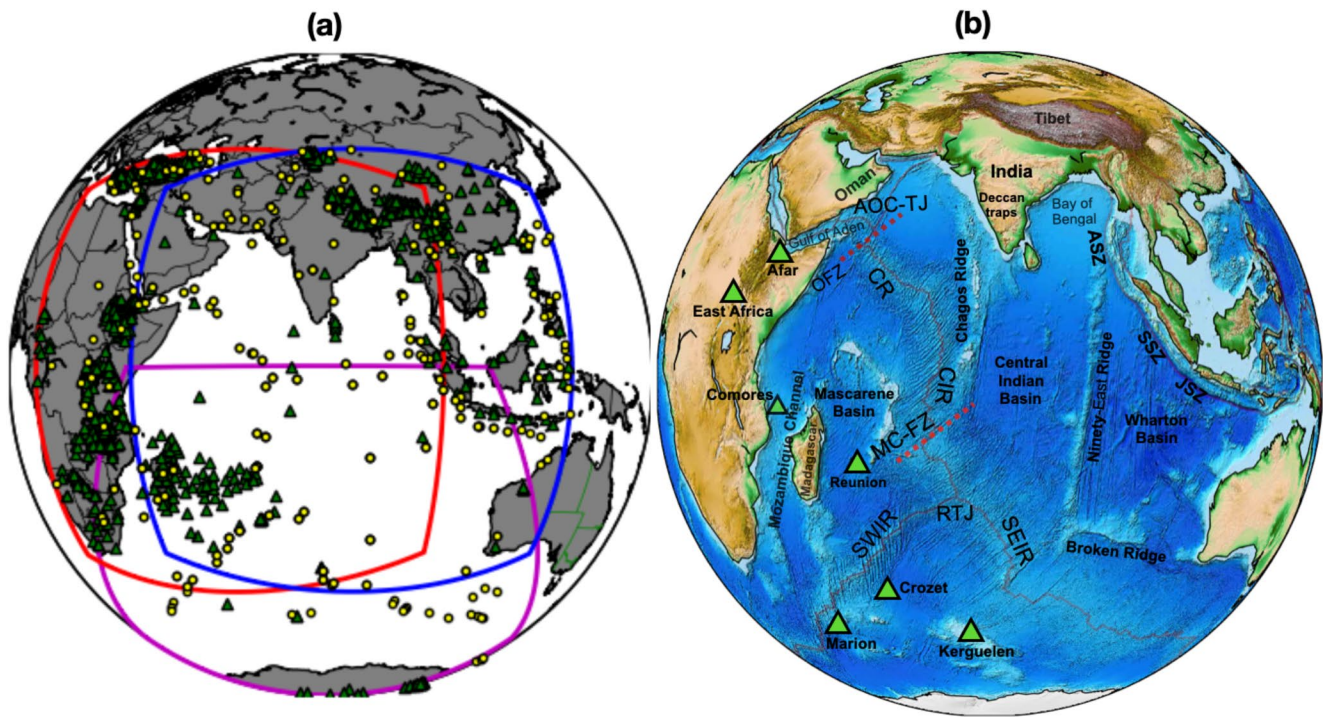


**Figure 1.** (a) Location map of seismic events (yellow dots) and seismic stations (blue triangles) used in this study, in the overlapping three RegSEM chunks (red, blue, and magenta lines) allowing to include teleseismic events at larger distance. Our data set comprises 200 events and 414 seismic stations, including 57 Ocean Bottom Seismometers from the RHUM-RUM experiment around La Réunion hotspot. (b) Bathymetric map of the Indian ocean showing various geological features. Green triangles represent hotspots, the red dashed lines indicate particular fracture zones: Owen Fracture Zone and the Marie Celeste Fracture Zone. Two triple junctions are located on the map: Aden-Owen-Carlsberg Triple Junction in the Northwest and Rodrigues Triple Junction in the South of the ocean. Mid-ocean ridges are represented by gray lines: Southwest Indian Ridge, Southeast Indian Ridge, Central Indian Ridge, Carlsberg Ridge. The Eastern subduction zones are indicated by Andaman subduction zone, Sumatra subduction zone and Java subduction zone.

Backus (1962), Capdeville and Marigo (2007), S. French and Romanowicz (2014). Here, we do not update the first 60 km of the model, which includes the crust, because our waveforms have weak sensitivity in that depth range. The crustal model is therefore the same as that of SEMUCB-WM1, for the construction of which dispersion data between periods of 20 and 150 s period were used jointly with waveforms to constrain the shallow part of the upper mantle (S. French & Romanowicz, 2014).

For the inverse part of the process, we follow the Bayesian optimization approach of Tarantola and Valette (1982) assuming slight non-linearity and Gaussian statistics. We use a Gauss-Newton least squares optimization approach of Tarantola and Valette (1982) as opposed to a pre-conditioned gradient method as used in adjoint-based inversions (Tarantola, 1984; Virieux & Operto, 2009). We construct the approximate gradient and Hessian, using physics-based normal mode perturbation theory, specifically the path-average approximation (PAVA) (Woodhouse & Dziewonski, 1984) for the fundamental mode surface waves, and non-linear asymptotic coupling theory (NACT) (Li & Romanowicz, 1995; Romanowicz et al., 2008) for overtone wavepackets. The latter takes into account coupling across mode branches and leads to 2D sensitivity kernels in the vertical plane containing the source and the receiver. Both PAVA and NACT contain multiple-forward scattering terms that take into account path-specific updates of the model in the calculation of the Fréchet derivatives. It is very important to calculate the Hessian, as it reduces the number of iterations for convergence. The model is updated using Equation S.2 in supporting information, where the data covariance matrix  $C_d$  is built from the weights applied to the individual wavepackets as described below and in Li and Romanowicz (1995). In building the gradient and Hessian, we also apply different weights to different subsets of data, to balance the contribution to the Fréchet derivatives of transverse component data versus data recorded on the vertical/longitudinal components and balance the contribution of overtones as compared to fundamental modes (Li & Romanowicz, 1996). The a priori model covariance matrix  $C_m$  provides



**Figure 2.** Path coverage for the entire data set used in our study. It comprises about ~1500 intersecting paths across Indian Ocean, with the densest coverage around the island of La Réunion.

for regularization of the model. In addition to norm damping, we consider lateral and depth correlation lengths as follows:

$$\mathbf{C}_m(\mathbf{r}_i, \mathbf{r}_j) = \sigma_{ii}\sigma_{jj} \exp\left(\frac{\cos\Delta_{ij} - 1}{L_{ij}^2}\right) \exp\left(\frac{-r_{ij}^2}{2h_{ij}^2}\right) \quad (1)$$

$\Delta_{ij}$  is the minor arc distance between model parameters  $i$  and  $j$ ,  $r_{ij}$  is the radial distance between them,  $L_{ij}$  are the lateral and  $h_{ij}$  the depth correlation lengths.  $\sigma_{ii}\sigma_{jj}$  are the a priori parameter uncertainties and include the norm damping factor (they are defined as the classical ranges of variations of elastic parameters as derived from a typical temperature field and rotations of the elastic tensors of models such as pyrolite and piclogite). The choice of the correlation lengths  $L_{ij}$  is dictated by the path coverage density in order to get a stable model without spurious small scale fluctuations. The expressions of the partial derivatives are derived from those of the seismograms in the PAVA and NACT formalism, (supporting information, Section 1). More details can be found in Lekić and Romanowicz (2011). The whole workflow of our inversion is presented in supporting information (Figure S8).

#### 4. Model Parametrization

The spatial parametrization of the model perturbation  $\delta m(r, \theta, \varphi)$  is defined by using spherical splines (Wang & Dahlen, 1995) for lateral parametrization and cubic splines for radial parametrization (Figure 4) spanning the depth range 30–2,900 km

$$\delta m(r, \theta, \varphi) = \sum_q \sum_p m_{qp} B_q(r) S_p(\theta, \varphi), \quad (2)$$

where,  $\theta$ ,  $\varphi$  are respectively the latitude and longitude, and  $r$  the radius.  $S_p(\theta, \varphi)$  and  $B_q(r)$  are respectively the spherical and cubic splines, and  $m_{qp}$  are coefficients defining the model perturbation at each iteration. The spherical spline basis has the advantage of being a local basis contrary to commonly used spherical harmonics. The lateral resolution of the model is not only limited by the spherical knot spacing which is chosen to be  $2^\circ$  (Figure 4), but it also depends on the path coverage, the frequency range of the waves, and

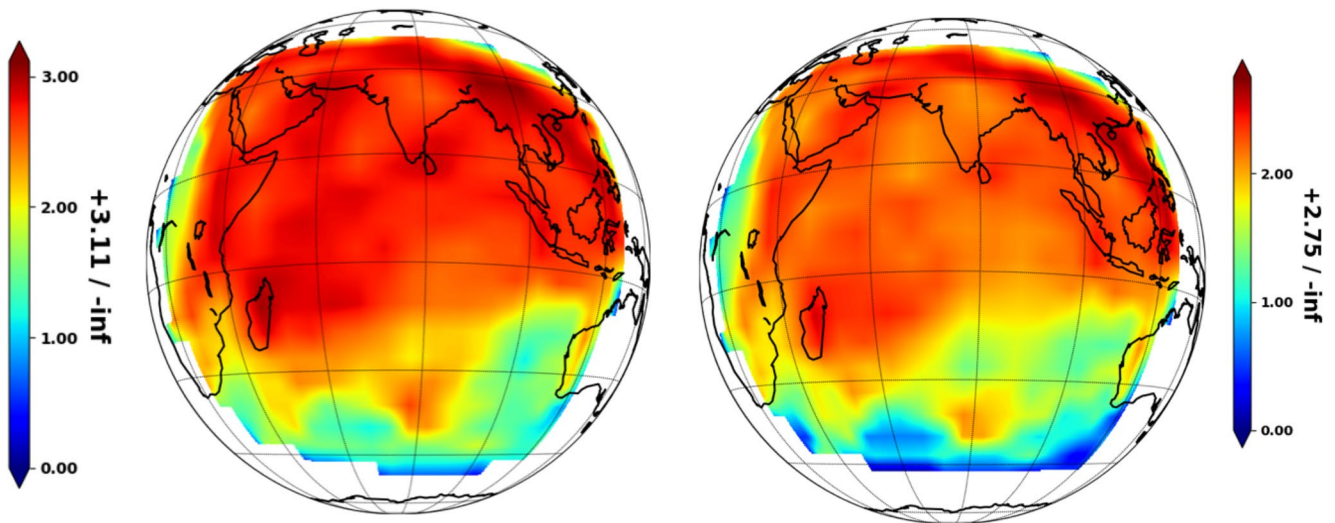


**Figure 3.** Hit count map (in logarithmic color scale, the hits are counted within the mesh of  $0.5^\circ \times 0.5^\circ$ ) for fundamental, higher and mixed modes of Rayleigh (left) and Love waves (right). The red (resp. blue) areas correspond to regions where the path coverage is the denser (resp. poorer). The whole region is better sampled by Rayleigh waves than by Love waves.



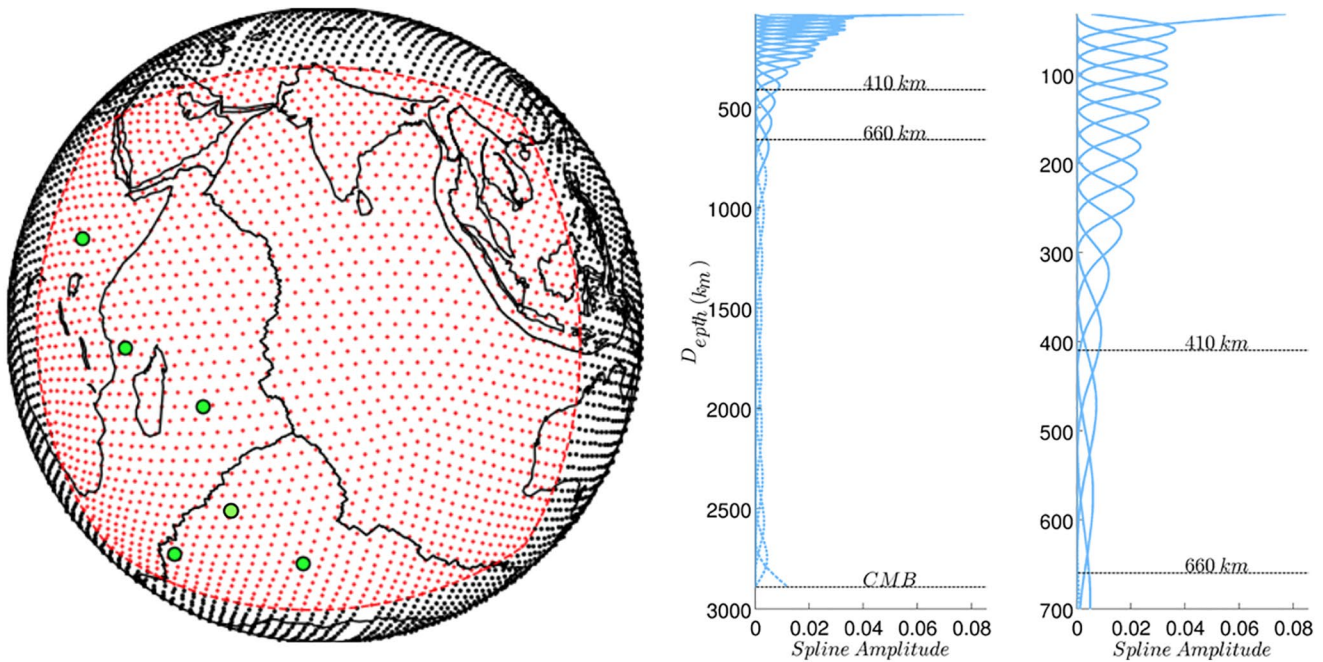


**Figure 4.** Left: Spherical spline node distribution with node spacing of  $2^\circ$ . The red dots delimited by the dashed red line represent the nodes that fall in the region of interest. The green circles are hotspots in the region of interest. For this region, we used the same node spacing for  $V_s$  and for  $\xi$ . Right: cubic-splines used for the vertical parametrization (with zoom from 100–700 km showing the distribution of cubic splines in the upper mantle transition zone). The radial nodes are unevenly spaced, tight in the uppermost mantle and loose with increasing depth, following the varying radial resolution.

the smoothing and damping applied in the inversion. Note that in this study, we update the model only down to 1,200 km depth.

For the physical parametrization, we consider the Earth as a transversely isotropic medium with a vertical axis of symmetry. Such a medium is described by the five Love parameters  $A, C, F, L, N$  (Love, 1927) plus density  $\rho$  defined in supporting information (Section 3) or alternatively two Voigt average isotropic velocities ( $V_{Piso}$ ,  $V_{Siso}$ ) and three anisotropic parameters,  $\xi$ ,  $\phi$  and  $\eta$  as defined in supporting information (Section 4). Here we only invert for  $V_{Siso}$  and  $\xi$  due to the fact that the parameters  $V_{Piso}$ ,  $\phi$ ,  $\rho$ , and  $\eta$  are usually not well constrained by long period waveforms. For these parameters, we use the scaling laws from Montagner and Anderson (1989), given in supporting information (Section 5).

## 5. Deep Structure Beneath the Indian Ocean Inferred From Waveform Inversion

The 3D regional tomographic model (SEMINDO) presented here has been obtained after three iterations of inversion, starting from model SEMUCB-WM1, which is a global model in which the parametrization of isotropic velocity ( $V_s$ ) and the radial anisotropy ( $\xi$ ) was done with spherical splines of different levels (e.g., level six for  $V_s$  and level 4 for  $\xi$ ), compared to the present parametrization (level six for both  $V_s$  and  $\xi$ ). Figure 5 shows a comparison of the average 1D model in Versus and  $\xi$ , compared to the global average in SEMUCB-WM1. Because the region is oceanic, the 1D reference Earth model remains close to the starting global average. However, the peak in  $\xi$  at 150 km depth is more pronounced in the final model.

### 5.1. Upper Mantle Down to 410 km

Figures 6 and 7 present the corresponding shear-wave-velocity ( $V_s$ ) maps from 100–150 km and from 200–400 km depth respectively, compared to the starting model SEMUCB-WM1 (on the left). At 100 km depth, our model features the well known low-velocity structures associated with mid-ocean ridges, from the Red Sea and the Gulf of Aden in the North, to the Carlsberg, Central and the South-East Indian ridges.

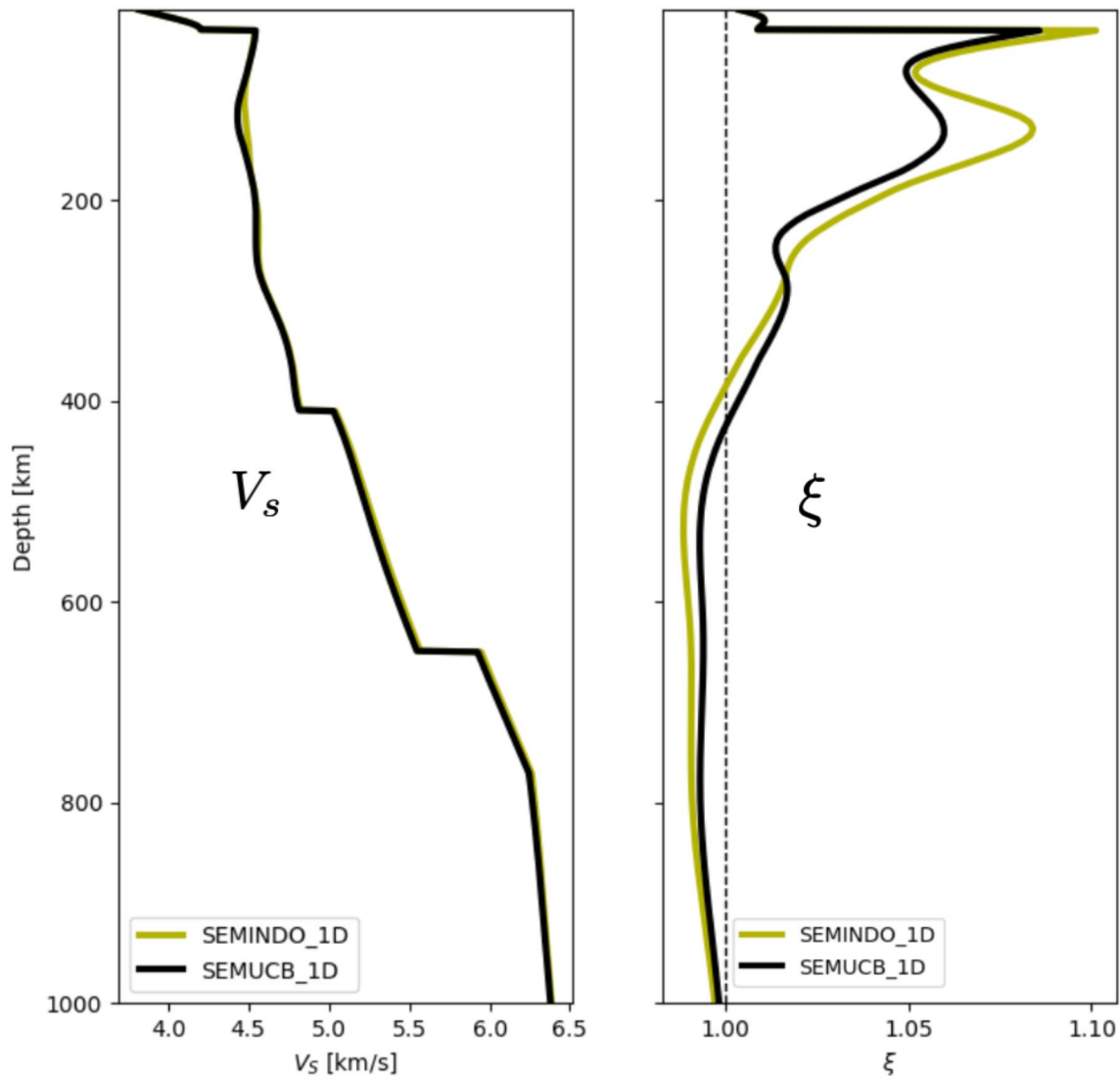


**Figure 5.** Comparison of mean isotropic velocity of the starting model SEMUCB-WM1 (black) and updated model SEMINDO (yellow) on the left, as well as radial anisotropy (right). Radial anisotropy is defined as  $\xi = V_{SH}^2 / V_{SV}^2$ .

Interestingly, the ultra-slow South West Indian Ridge (SWIR) is not associated with continuous low-velocities at these depths except in its SW part, which might be related to Marion hotspot. This is consistent with the dynamics of this region, and with previous findings (Montagner, 1986; Sauter et al., 2009). More recently (Debaille & Ricard, 2012; Mazzullo et al., 2017) also show the absence of pronounced low-velocities beneath the SWIR. At 150 km depth, that is, at asthenospheric depths, the tomographic model indicates that the continuous signature of the ridges has disappeared. We note, however a prominent low-velocity anomaly on the western side of the CIR (Central Indian Ridge) (marked *M* on Figure 6) and low velocity anomaly of larger spatial extent on the eastern side of CIR (marked *C* on Figure 6). Anomaly *M* extends southward to the Réunion, and westward to the Comoros archipelago. This anomaly corresponds well to the structure called MBAR (Mascarene Basin Asthenospheric Reservoir), imaged by fundamental mode Rayleigh wave tomography (Barruol et al., 2019; Mazzullo et al., 2017). In our regional model SEMINDO, the MBAR anomaly extends down to ~250 km depth but vanishes in the underlying upper mantle transition zone. Anomaly *C* extends in a large part of the Central Indian Ocean Basin and eastward to the Sumatra and Sunda subduction zones. We name it the Central Indian Ocean Basin Anomaly (CIOBA). This anomaly is visible down to the transition zone though weaker below 300 km depth. Figure 6 (right panel) shows that the thickness



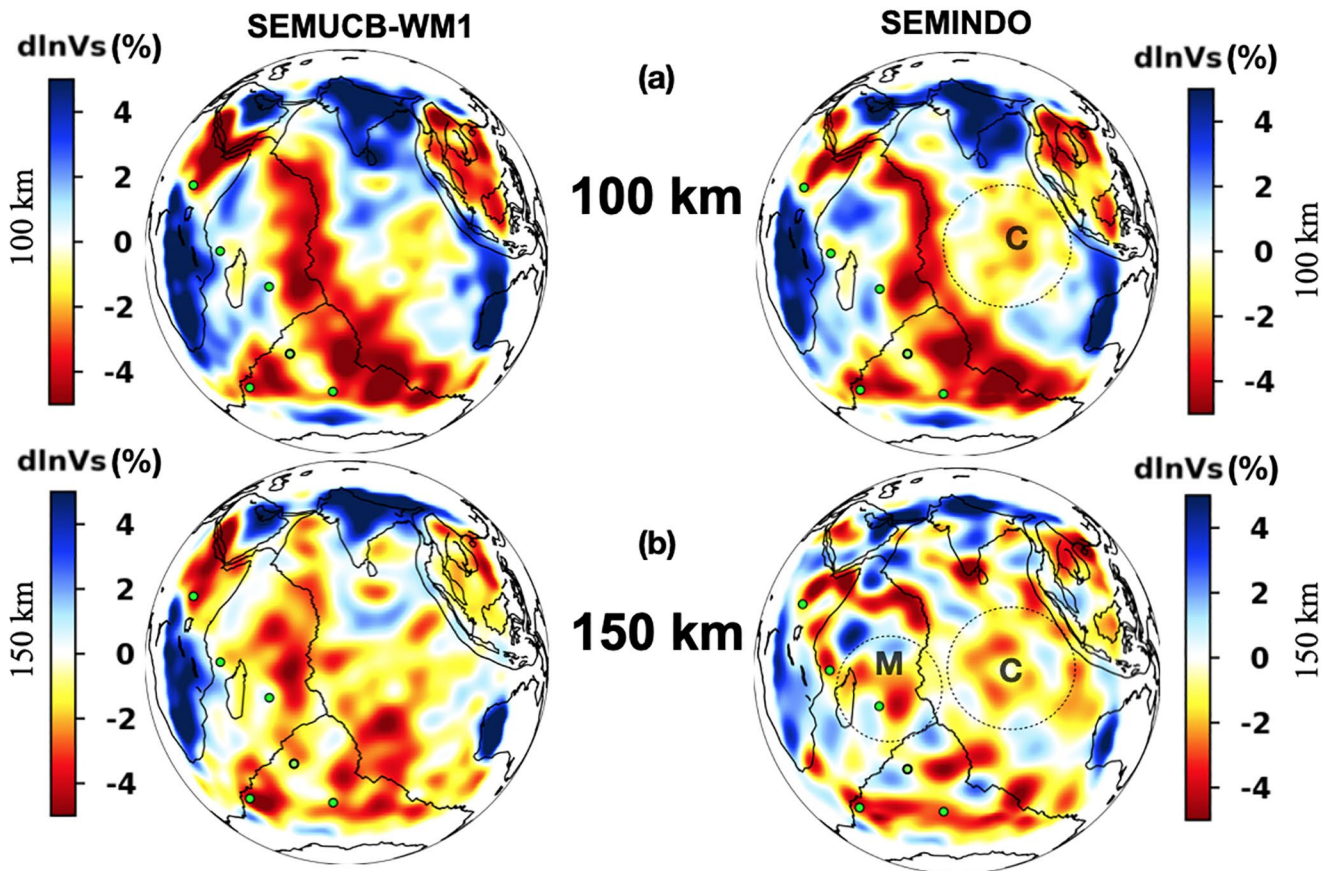


**Figure 6.** Comparison of the  $V_{Siso}$  distribution in the starting model (SEMUCB-WM1) on the left, and the updated model (SEMINDO) on the right at depth of 100 km (a), and at 150 km depth (b). The shear-wave-velocity perturbation is plotted relative to the regional averages plotted on the left column of Figure 5. The low velocity anomalies located on the left and right-hand side of the Central Indian Ridge in SEMINDO are highlighted by dashed circles at 150 km depth and are labeled *M* (stands for Mascarene Basin anomaly, also MBAR) and *C* (stands for Central Indian Ocean Basin anomaly, also CIOBA), the latter anomaly is also significant at 100 km depth. The low-velocity anomalies located in the SW corner of the Southwest Indian Ridge and in the south of the Indian Ocean correspond to the Marion and the Kerguelen hotspots, respectively. Green dots represent hotspots.

of the fast Indian continent lithosphere varies geographically. The fast velocity Indian keel anomaly clearly shows up (Figure 6b) and is in good agreement with the tomographic model of (Maurya et al., 2016). At 150 km depth, a very slow anomaly is present at the southern tip of India. As shown at 300 km depth (Figure 7b, right panel) it may be connected to a continuous and broad low-velocity body extending NE from Seychelles to the South of the Indian continent. This elongated low velocity body aligned with the absolute plate motion has many similarities with a finger-like structure observed in the Pacific ocean by (S. French et al., 2013). Although it is still visible at 400 km depth, its signature is considerably weaker and vanishes in the transition zone (as will be seen in the next section Figure 8).

## 5.2. Transition Zone and Lower Mantle

The joint inversion of fundamental and higher modes is useful to image deeper structure than was possible in the previous tomographic modeling based on fundamental mode Rayleigh waves (Mazzullo et al., 2017), and to better constrain the roots of these anomalies. It also makes it possible to retrieve the structure in the transition zone and in the upper part of the lower mantle. Interestingly, the CIOBA slow structure is still visible in the upper mantle transition zone (i.e., 410–660 km depth), and in the uppermost lower mantle (Figures 8a–8c), and resolved (supporting information, Figure S6 for the resolution tests). From the upper mantle down to the transition zone, the CIOBA is always bordered on its eastern side by the Sumatra or Sunda subduction zones (Figures 7 and 8). On the other hand, the MBAR anomaly starts to weaken at

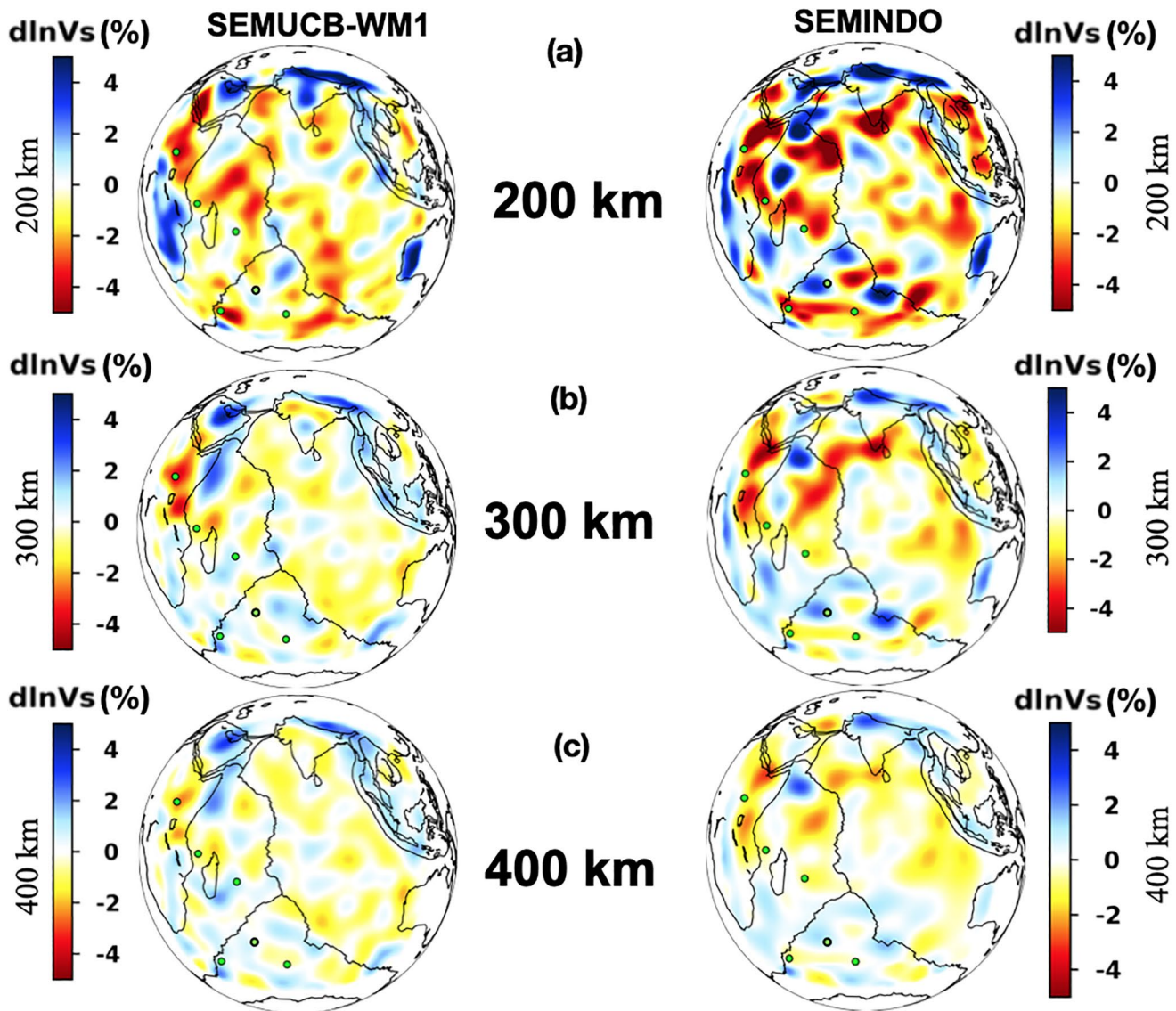


**Figure 7.** Comparison of the  $V_{siso}$  distribution in the starting model (SEMUCB-WM1) on the left panel, and the regional model (SEMINDO) on the right panel at depths of 200 km (a), 300 km (b) and 400 km (c). The shear-wave-velocity perturbation is plotted relative to the regional average with the same color scale on all panels. In SEMINDO, the overall amplitudes of the anomalies decrease with depth but their signatures are still visible at the base of the asthenosphere at 400 km depth.

~250 km depth and completely disappears at ~550 km depth (Figure 8a, right panel). Only a low amplitude low-velocity anomaly remains beneath the Réunion hotspot.

Similar patterns of low and fast velocity anomalies are visible from 650 km down to 1000 km (Figure 8, right panel) with decreasing amplitudes with depth. The dominant low-velocity anomalies located beneath the Réunion hotspot and those associated to the CIOBA are visible down to 1000 km depth (Figure 8). Between them, from 650 to 1000 km depth, a positive (fast) velocity anomaly extends from just south of the Aden-Owen-Carlsberg Triple Junction (northern triple junction in the Indian Ocean, indicated in Figure 1b as AOC-TJ) to the northern part of the SEIR (Figure 8). It likely represents the remnant of the Carlsberg slab, arising from the oblique subduction of Indian lithosphere beneath the Arabian/African oceanic lithosphere during the late Cretaceous to Paleocene (Hafkenscheid et al., 2006). The low-velocity anomaly beneath the Indian continent visible in the starting model SEMUCB-WM1 at 550–800 km depth (Figure 8, left panel) is no longer visible in SEMINDO at these depth ranges.



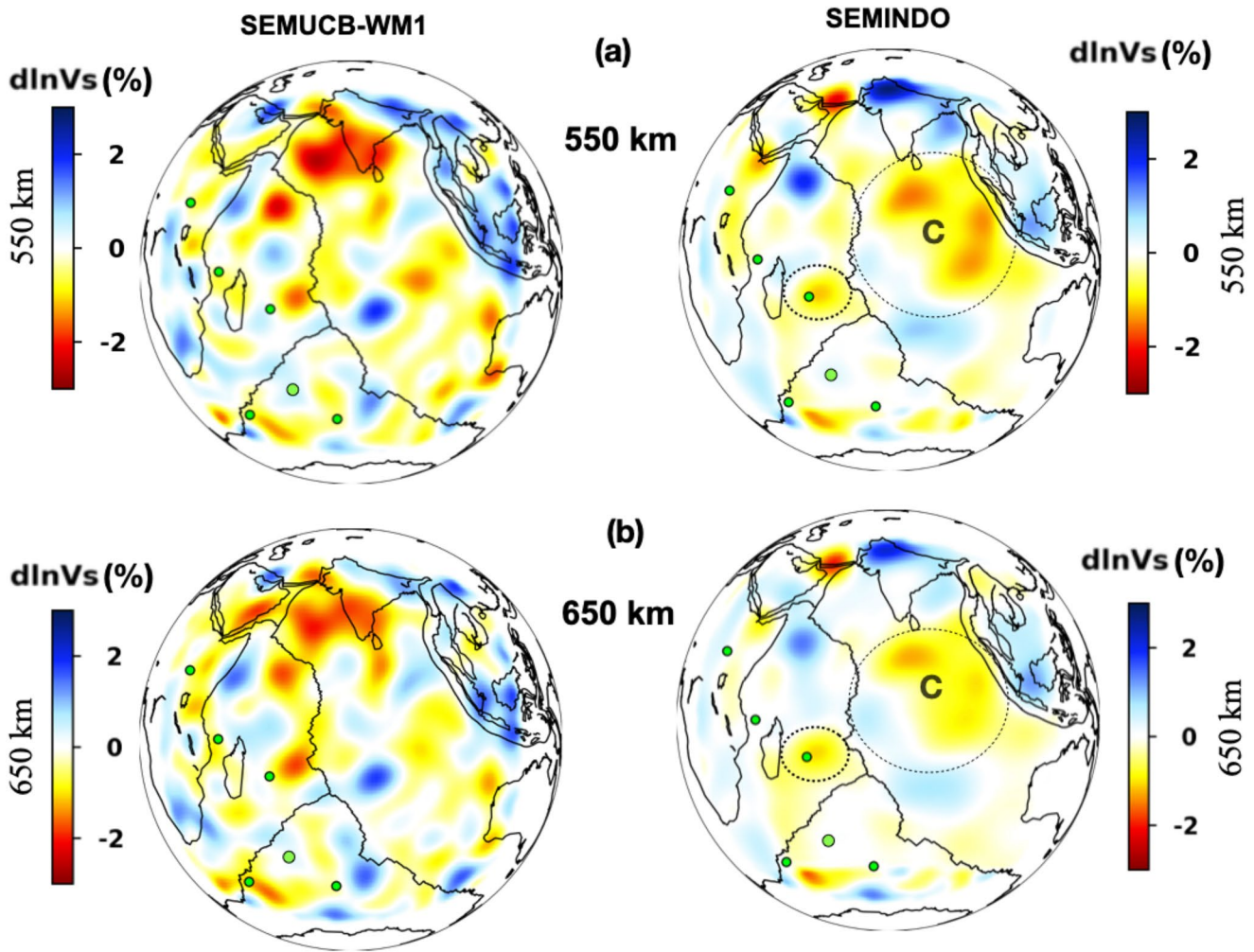


**Figure 8.** (continued)  $V_{Siso}$  distribution in both SEMUCB-WM1 (left panel) and SEMINDO (right panel) models in the transition zone and uppermost lower mantle at 550 km (a), 650 km (b), 800 km (c) and 1000 km depth (d). Due to the decrease of amplitude with depth, the models are plotted with a different color-scale ( $\pm 3\%$  from 550–650 km and  $\pm 2\%$  from 800–1000 km) than the one used in Figure 7, for the upper mantle structure. The low-velocity structures on the Eastern side of the Central Indian Ridge (indicated by C - meaning Central Indian Ocean Basin Anomaly - surrounded with a dotted circle) is still visible in the transition zone, and spreads eastward at 550–800 km depth as visible on the right panel.

### 5.3. Comparison Between the Shear-Velocity and Radial Anisotropy Parts of the Model

The radial anisotropy  $\xi$  is retrieved from the joint inversion of Rayleigh and Love waves. To first order, radial anisotropy is dominated by horizontal flow prevailing in oceanic basins and layering with  $\xi > 1$ . We remove the regional average  $\xi_{ref}$  before plotting maps of radial anisotropy perturbations ( $\delta\xi = \xi - \xi_{ref}$ ). The radial anisotropy maps (Figures 9 and 10) display a strong anisotropy down to 200 km depth, decreasing at larger depths, which is in good agreement with results from other oceanic basins. However, we also observe in SEMINDO beneath most Indian ocean hotspots (La Réunion, Kerguelen, Marion) and the East African rift that  $\delta\xi < 0$ , likely indicating mantle upwellings beneath these areas (Figures 9 and 10, right panel). Although certain hotspots (Crozet and Comores) less than the average still display positive radial anisotropy  $\delta\xi > 0$  at 200–300 km depth. An ( $\delta\xi < 0$ ) elongated region is also observed between the Carlsberg ridge and South India which might be related to the finger-like structure also observed in  $V_S$  model at 300 km depth.

As shown in Figure 10 (SEMUCB-WM1, left panel), these small-scale features beneath hotspots could not be resolved in the global scale tomographic model SEMUCB-WM1. The smaller grid-spacing ( $\leq 2^\circ \times 2^\circ$ ) used for radial anisotropy parametrization (as well as shear-wave velocity), combined with improved data coverage, allows to recover shorter wavelength structures in the regional model (Figures 9, 10b and 10c,

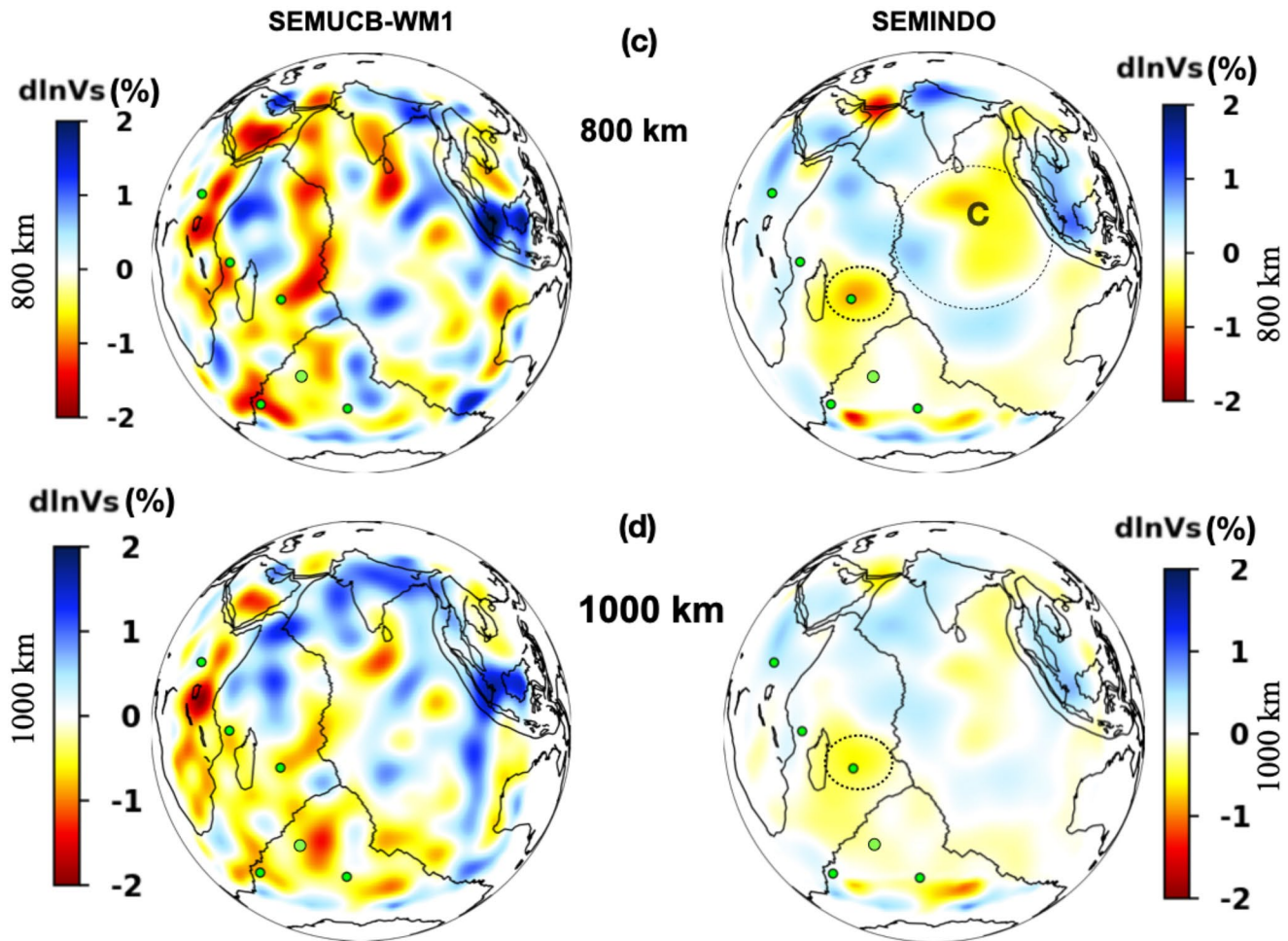


Figure 8. Continued.

right panel). The fast velocity anomalies near Aden-Owen-Carlsberg triple junction (indicated on Figure 1b as OAC-TJ) and around the SWIR also have corresponding anomalies in radial anisotropy ( $\delta\xi > 0$ ) at 200, 300 km depth (Figure 9, right panel). We do not present the radial anisotropy part of SEMINDO below 400 km depth, since its amplitude is quite small. Even if present, radial anisotropy amplitude is within the error bars for depths  $\geq 400$  km, as shown in the supporting information (Figure S7).

#### 5.4. Deep Mantle Structure Beneath the Réunion Hotspot

In order to determine the origin at depth of the various structures beneath the Réunion hotspot, we plot several depth cross-sections around it along different orientations (Figure 11). In these cross-sections we merge our model (SEMINDO) above 1200 km depth, with the background model (SEMUCB-WM1) beneath 1200 km depth, since our inversion extends only down to  $\sim 1200$  km. This allows us to gain insights on possible connections with the Large Low Shear-Velocity Province (LLSVP) at the base of the lower mantle. The color-scale is adapted in such a way that the lower mantle features are emphasized by saturating it at  $\pm 2\%$  in the upper mantle and at  $\pm 1\%$  in the transition zone and in the lower mantle. The fast velocity observed in the uppermost mantle beneath Réunion in SEMUCB-WM1 (Figures 11a and 11b) is no longer present in our model SEMINDO (Figures 11e and 11f), which instead shows evidence of continuous low-velocity structure with depth, broadening in the transition zone and thinning again in the uppermost lower mantle. The Mascarene Basin reservoir also appears to be connected to the lower mantle through the same plume conduit (Figure 11f, right panel). The size ( $< 800$  km) of the plume conduit in the lower mantle beneath



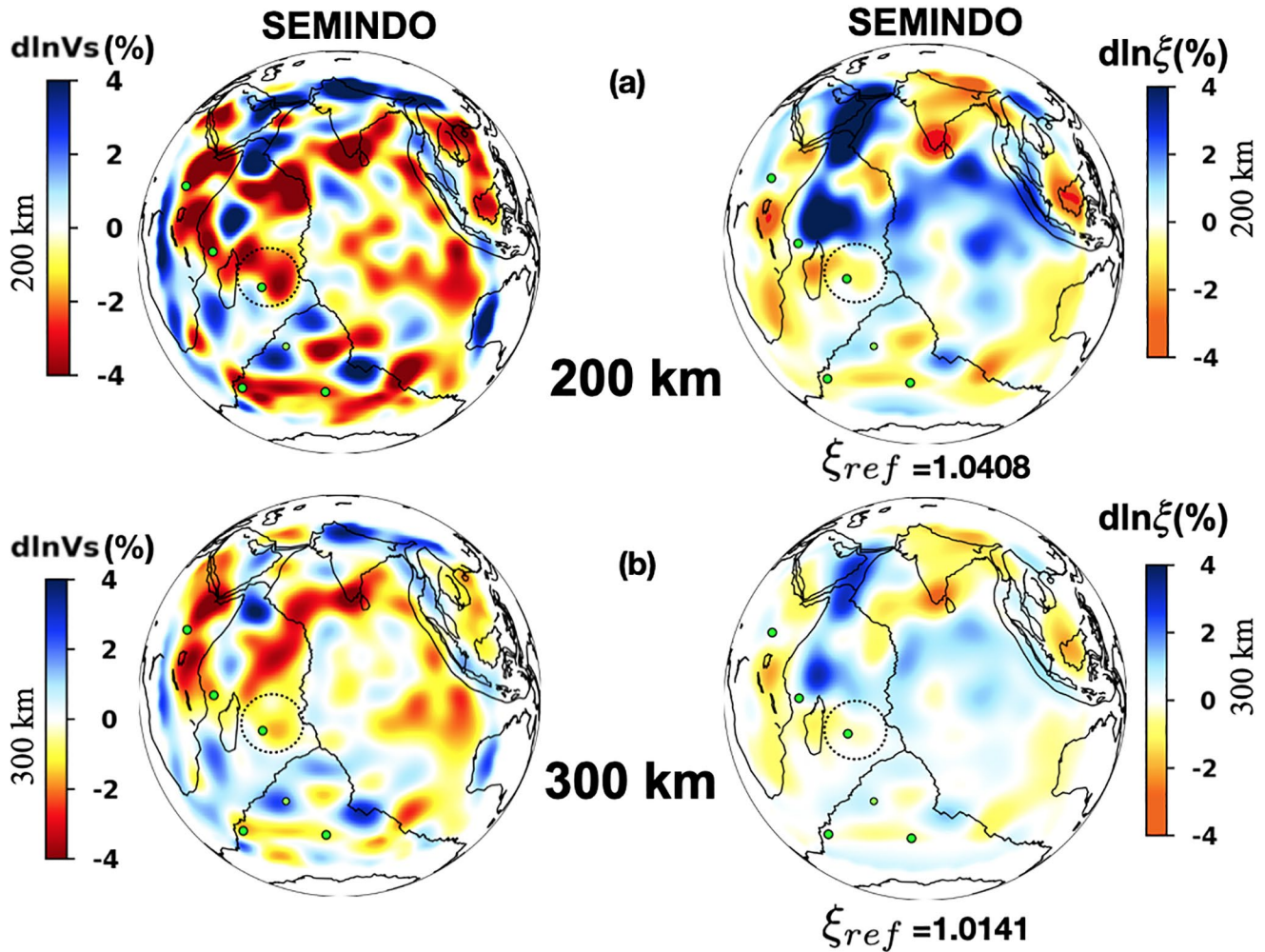


**Figure 9.** Comparison between the isotropic velocity (left panel) and the radial  $d\ln \xi$  anisotropy (right panel) parts of the model at depths of 200 km (a) and 300 km (b). Both are resolved on the same grid (with spacing of  $2^\circ \times 2^\circ$ ). The radial anisotropy is plotted relative to the reference value at the corresponding depth, which is  $\xi_{ref} = 1.0408$  at 200 km depth and  $\xi_{ref} = 1.0141$  at 300 km depth. The elongated region (characterized by  $\delta V_s < 0$  and  $\delta \xi < 0$ ) between the Carlsberg ridge and the south of the Indian continent is well represented in  $V_s$  and  $\xi$  models at 200 and 300 km depth.

Réunion is smaller than those of Hawaii, Pitcairn and Samoa as shown in SEMUCB-WM1. In addition to the new data set from RHUM-RUM experiment, the improved coverage of the Indian Ocean may explain why this conduit was not resolved in the starting model (S. W. French & Romanowicz, 2015) nor in other tomographic models (Figure 12).

We observe a low-velocity anomaly that rises from lower mantle and spreads in the uppermost mantle (Figures 11e–11h). A conduit with weak amplitude in the lower mantle appears clearly in SEMINDO as well as in SEMUCB-WM1 (Figure 11). The conduit is very similar in both models at  $\sim 1200$  km depth, which is the limit of depth resolution of our inversion. The conduit in SEMINDO model (Figure 11, right panel) links the Réunion hotspot to the South Africa LLSVP (belonging to the non-inverted part) as well as to the base of the mantle beneath the southern Indian Ocean in the neighborhood of the Kerguelen hotspot (Figures 11a). This conduit could represent mantle upwelling related to the discharge of the LLSVP content in the upper mantle or to the viscosity contrast between the upper and lower mantle. The fast velocity anomalies visible on the two cross-sections (Figures 11g and 11h) are likely related to the history of the Sunda subduction zone and the Carlsberg slab respectively.

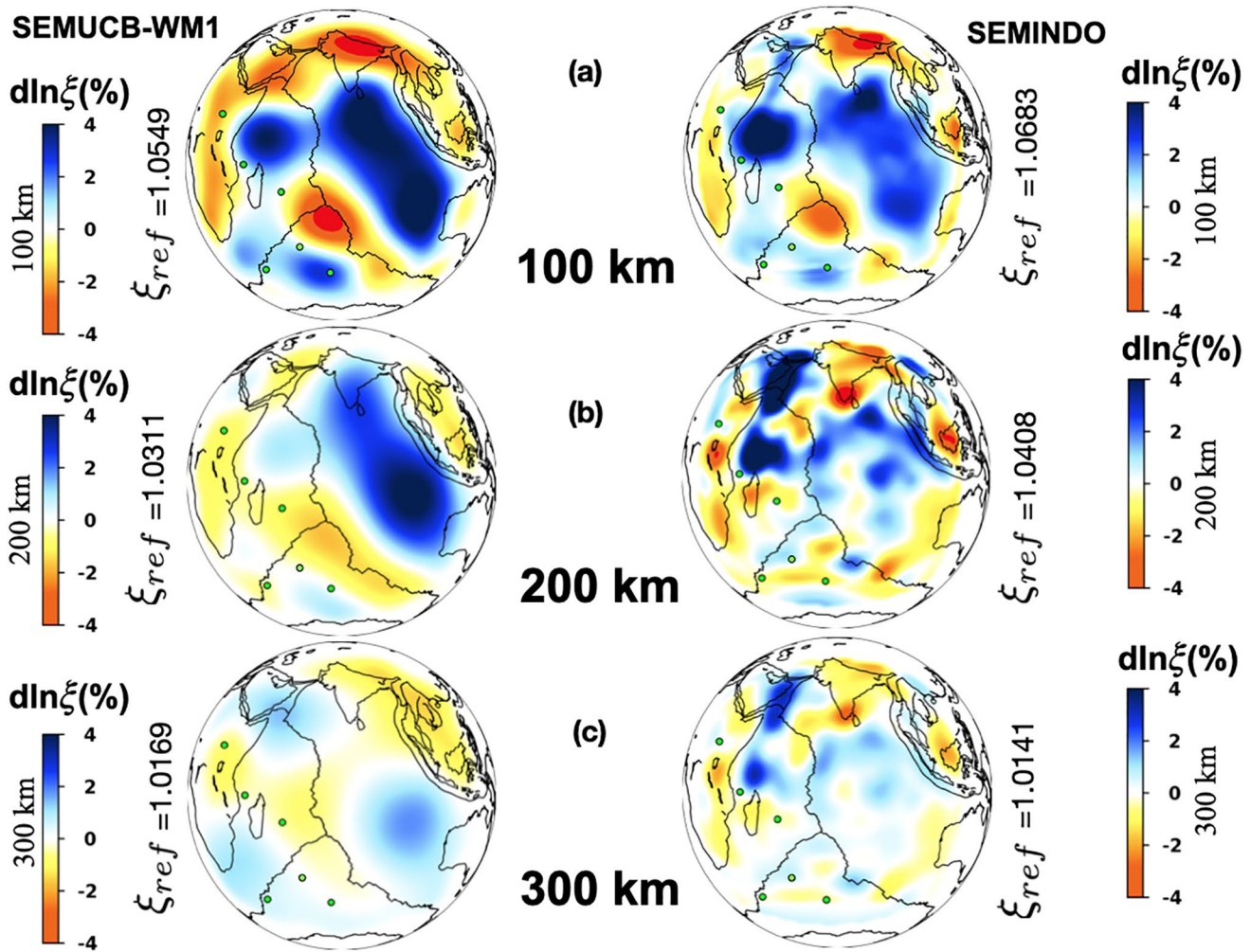


**Figure 10.** Comparison of radial anisotropy of SEMUCB-WM1 model (left panel) and of our study (right panel), at depth of 100 km (a), 200 km (b) and 300 km (c), showing overall similar amplitudes but features of smaller wavelength. The reference values ( $\xi_{ref}$ ) at each depth are shown on the figure.

## 6. Discussion

In this section, we compare SEMINDO to other models and discuss the potential origin of slow and fast velocity anomalies that we resolve in the Indian Ocean, from the upper mantle down to the mid-lower-mantle.

### 6.1. Comparison With Other Models

Since 1986, several surface wave regional tomographic models have been developed to image the mantle structure beneath the Indian Ocean. The first model used 86 ray paths to perform an inversion of Rayleigh wave dispersion (with the period range of 40–300 s) by Montagner (1986), followed by a model using 156 surface waveforms of Rayleigh and Love waves (Debayle & L  v  que, 1997). In the asthenosphere, both models found low-velocity anomalies on either side of the CIR and the fast velocity anomaly near the Aden-Owen-Carlsberg Triple Junction (Figure 2d in Debayle & L  v  que, 1997). The most recent surface wave tomography (focused around La R  union) including the RHUM-RUM data (Mazzullo et al., 2017) better constrained the geometry and anisotropy of the MBAR anomaly located beneath the Mascarene Basin. Many other studies used joint seismic-geodynamic-mineral physical modeling, and seismic azimuthal anisotropy derived from shear wave splitting, to investigate asthenospheric flow beneath the Indian Ocean (Barruol et al., 2019; Forte et al., 2010; Scholz et al., 2018). These studies reached a consistent conclusion, highlighting the presence of a W-E flow beneath the SW Indian Ocean at asthenospheric depth. In



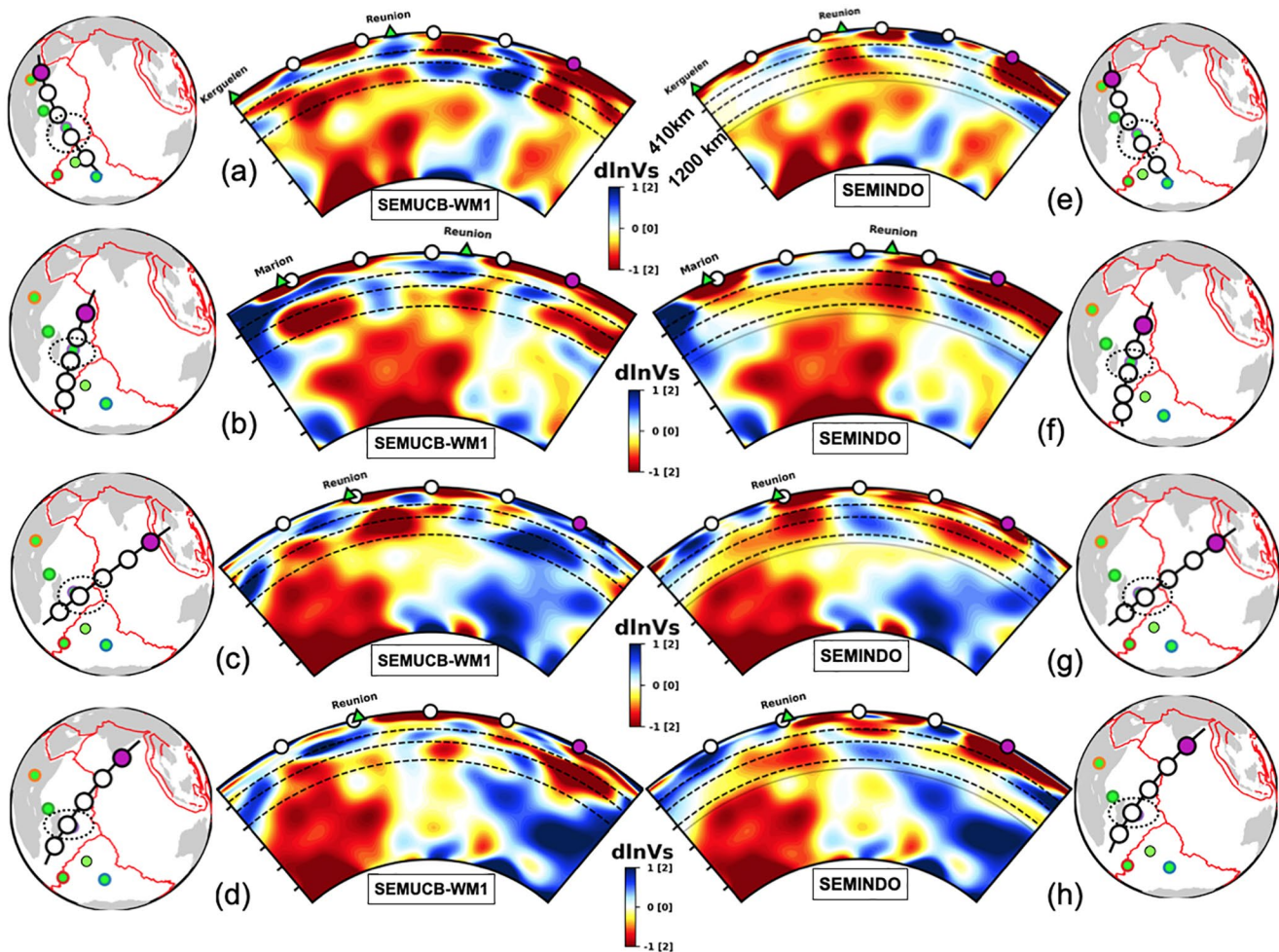


**Figure 11.** Comparison of whole-mantle cross-sections in SEMUCB-WM1 (left panels) and SEMINDO (this study, right panels) around the Réunion hotspot from different viewing angles. The two models are identical below 1200 km depth, since the inversion for SEMINDO was performed only down to that depth, indicated by the continuous gray line on the right hand side cross-sections. The deepest part of SEMINDO is still influenced by SEMUCB up to ~200 km. Dashed lines indicate depths of 410, 660 and 1000 km. In SEMINDO, we resolve smaller-scale features beneath Réunion and Marion hotspots. The color scales in the upper and lower mantle are respectively  $\pm 2\%$  and  $\pm 1\%$ . The latter color scale allows us to emphasize features in the transition zone and in the lower mantle.

our present regional tomography study, we inverted surface waves (fundamental mode plus higher modes) down to ~1200 km (which is the maximum sensitivity reached by our surface waveform data) giving us access to the structure beneath La Réunion down to the uppermost lower mantle. The model between this depth of 1200 km and the base of mantle (CMB) is the background model (SEMUCB-WM1) that remains unchanged. In Figure 12, we compare the model SEMINDO resulting from this study to other global models. This selection is rather arbitrary but representative of the variability of existing global tomographic models. The cross-sections shown in these models are: S40RTS from Ritsema et al. (2011); S362ANI from Kustowski et al. (2008) and SEMUCB-WM1 (S. W. French & Romanowicz, 2015). They display some common features (but also many differences) such as the low-velocity anomaly in the upper mantle ( $\leq 400$  km) and in the lower transition zone (660 – 1000 km) beneath the Réunion hotspot. An interesting feature visible from these various models is that low-velocities are observed in similar places in the transition zone, overlying similar small-scale conduits in the uppermost lower mantle linking to the LLSVP below. Model S40RTS (Ritsema et al., 2011) shows a trend of low-velocity anomaly from the lower to the upper mantle (Figures 12b and 12f). S362ANI from Kustowski et al. (2008) shows a low-velocity anomaly (Figures 12c and 12g) both in the uppermost mantle and the lower mantle, with a fast velocity anomaly between them, located in the transition zone. The two cross-sections from SEMUCB-WM1 (S. W. French

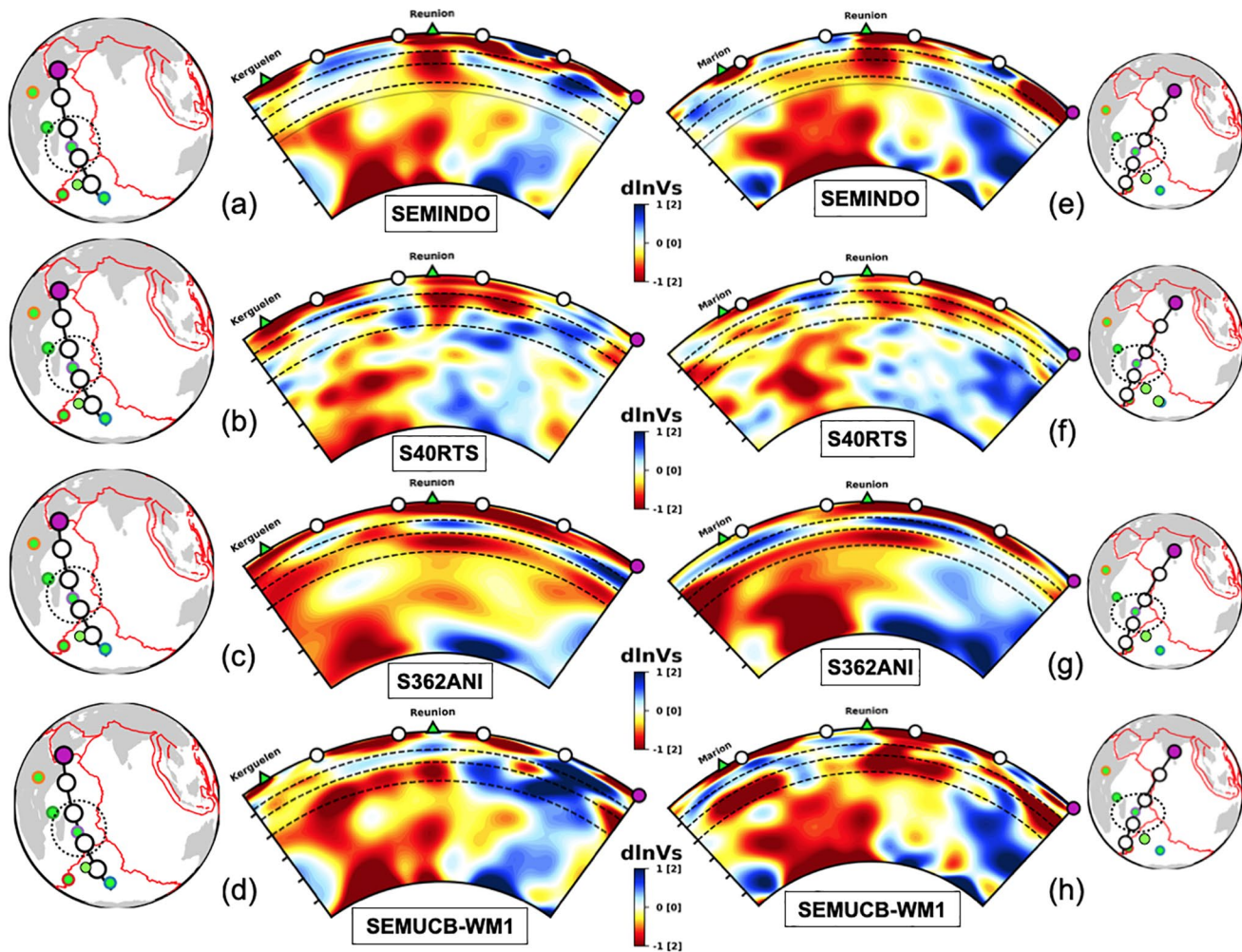


**Figure 12.** Comparison of SEMINDO model (upper panel) with models S40RTS from Ritsema et al. (2011); S362ANI from Kustowski et al. (2008) and SEMUCB-WM1 (S. French & Romanowicz, 2014) along two cross sections located on the map. All the models consistently show a similar low-velocity anomaly in the upper mantle or in the mantle transition zone beneath the Réunion hotspot. Models are less consistent beneath the Marion hotspot. S40RTS and SEMUCB-WM1 show a low-velocity trend from the lower to the upper mantle on both cross-sections. SEMINDO displays a continuous low velocity anomaly that may indicate a conduit connecting the Réunion hotspot to the lower mantle (a).

& Romanowicz, 2015) (Figures 12d and 12h) present a fast velocity anomaly beneath Réunion hotspot in the uppermost mantle (Figures 12d and 12h). In contrast, SEMINDO exhibits a continuous low-velocity structure across the whole upper mantle and the transition zone beneath the Réunion hotspot (Figures 12a and 12e), which may suggest a quasi-vertical conduit in these cross-sections.

The likely reason for discrepancies between global models results from the poor spatial coverage in the Indian Ocean with a very limited number of seismic sources and receivers, which implies a poor lateral resolution, whereas the addition of many earthquakes and data from temporary stations on land and on the seafloor, with the RHUM-RUM experiment, enables us to improve the lateral resolution beneath the Indian Ocean.

## 6.2. Origin and Source(s) of the MBAR and CIOBA?

The cross-sections presented in Figures 11f and 11g show that a good candidate to explain the observed anomalies in the upper mantle is a plume rising from the lower mantle and responsible for feeding the asthenosphere beneath the African and Indian lithospheres, and generating the MBAR (Figure 11f) and CIOBA (Figure 11g) anomalies. The MBAR appears to be connected to the lower mantle through a narrow



conduit beneath La Réunion. One can notice however, that all the cross-sections in (Figures 11f and 11h) show a low-velocity anomaly channel to the northeast of La Réunion (at depth of  $\leq 400$  km) trending toward the Central Indian Basin and connected to the conduit beneath the Réunion, in agreement with the so-called Rodrigues corridor (Barruol et al., 2019) documented from Rayleigh wave tomography and SKS shear-wave splitting (Mazzullo et al., 2017; Scholz et al., 2018).

In contrast, fast velocity anomalies are observed in the upper mantle southwest of the Réunion (Figures 11f and 11g) suggesting cold and thick lithosphere. The low-velocity anomaly in the Central Indian Basin (CIO-BA) seems to stagnate at  $\sim 700$  km in front of the Sunda slab sinking into the lower mantle (Figure 11g). The connection between the Mascarene Basin Asthenospheric Reservoir (MBAR), Comoros and East-Africa hotspots appears as a low-velocity channel in the uppermost mantle (Figure 9a, left panel). This asthenospheric channel may suggest the presence of a pressure gradient in the deep mantle that induces upper mantle flow. The connection between the two anomalies (MBAR and CIOBA) is not well established, and should be further investigated (for instance by performing an azimuthal anisotropy inversion down to the transition zone) to enlighten possible horizontal physical connection or independent feeding from below. Independent findings suggest that an increase of water content in the upper mantle supplied by lithosphere and sediment subduction can cause extensive zones of low-velocity in the upper mantle, as shown in the U.S. east coast by van der Lee et al. (2008). The low-velocity structure found beneath the Marion hotspot is more continuous (from the uppermost mantle down to 800 km, Figure 11f) than in the starting model, and may come from a plume deflection in lower transition zone (600–1000 km). Its resolution may be improved in the future by including body wave data in the inversion.

### 6.3. Possible Connections Between the Réunion, the Comoros and the MBAR?

From the maps presented in (Figure 7a, right panel), the low-velocity structure associated with the MBAR clearly links the Réunion in the South (at 200 km depth), the CIR in the East and the Comoros archipelago to the West (at 200 and 300 km depth). The major features visible on the cross-section shown in Figure 13a are first, the low-velocity structure that extends horizontally at asthenospheric depths and second, a plume conduit that connects the lower mantle to the Réunion hotspot. Figure 13b also exhibits well such a low-velocity anomaly channel between the Réunion, the Comoros and East Africa with a connection to the lower mantle in the vicinity of La Réunion.

The common observations on these two cross-sections are: (a) The vast spreading of the plume in the asthenosphere. (b) A plume conduit connecting the Réunion hotspot and the lower mantle. Observation (a) suggests a dominantly horizontal asthenospheric flow emanating from the Réunion hotspot, compatible with an increase of mantle plume flux beneath La Réunion, as proposed by Iaffaldano et al. (2018).

A truly radial flow pattern is, however, unlikely since a dominant WE azimuthal anisotropy culminating at about 150 km depth is evidenced by Rayleigh wave tomography (Barruol et al., 2019; Mazzullo et al., 2017). Observation (b) is present on most cross-sections and suggests a single source of mantle material rising toward the surface. Together, these features suggest that the upwelling plume could feed the asthenosphere by spreading northward to the Mascarene Basin, eastward to the CIR and westward to the Comoros. For Comoros volcanism, an alternative source might be provided by the East African rift (e.g., Michon, 2016). As proposed by Barruol et al. (2019), such large-scale, low-velocity anomaly trapped in the asthenosphere is probably derived from a mantle plume, the geometry and evolution of which remain to be defined, but that may look like an upwelling blob of hot material that became trapped beneath the thick and cold oceanic mascarene lithosphere and that spread with a predominantly horizontal motion.

### 6.4. Low-Velocity Conduits in the Lower Mantle?

The origin of volcanic hotspots and of the underlying mantle plumes has been controversial for several decades. Since Morgan (1971) proposed that plumes originate in the lowermost mantle, that is, at the core-mantle boundary (CMB), some alternatives have been proposed. From a geodynamical point of view, there seems to be a consensus that mantle plumes are induced by convective instabilities originating in thermal boundary layers. Consequently, it was proposed that different types of plumes might exist, originating from different mantle boundary layers, not only at the CMB but also in the mantle transition zone and

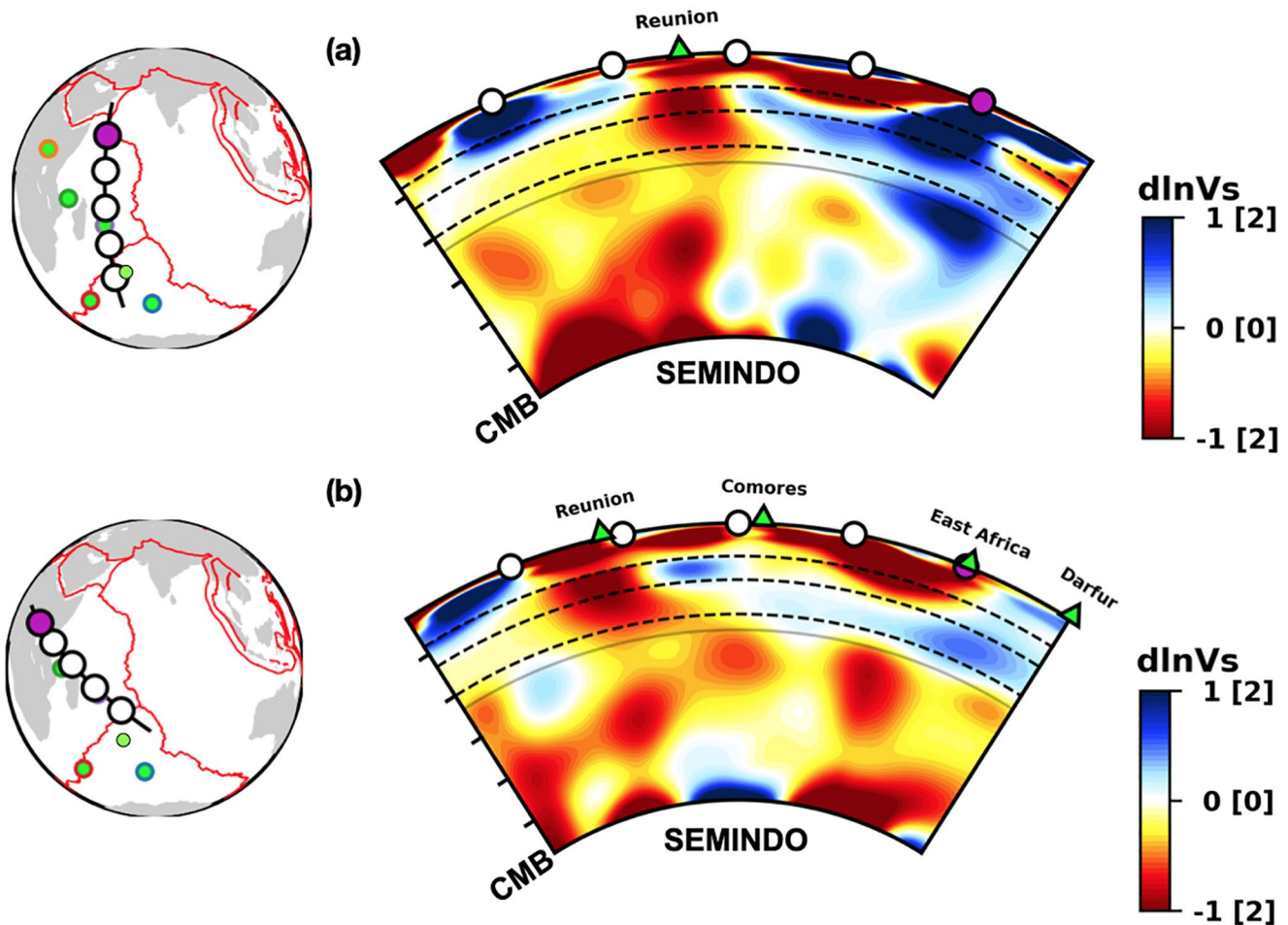


**Figure 13.** Sections across SEMINDO model: (a) Along a NS direction, connecting the Réunion hotspot and the Aden-Owen-Carlsberg Triple Junction. It exhibits a low-velocity anomaly beneath the Mascarene Basin, connected to the Réunion and rising from the lower mantle. (b) Along a SE-NW direction through the Mascarene Basin, Comoros and the East-Africa hotspots. This cross-section shows a low-velocity anomaly from the lower mantle, reaching the Réunion and spreading westward toward the Comoros and East Africa. The fast velocity anomaly in the corner top of the cross-section (a) may indicate the remnant Carlsberg slab. The dashed circles on the maps localize the Mascarene Basin (a) and the Comoros hotspot (b).

in the asthenosphere (Courtillot et al., 2003; Montagner & Ritsema, 2001) and the web site (<http://www.mantleplumes.org>). Some complexity arises when considering that mantle convection is not only thermal but also chemical, as thermochemical “domes” might exist in the lower mantle and generate rising instabilities feeding volcanic surface activity (e.g., Davaille et al., 2005). A good candidate for a thermochemical “dome” is the large low-velocity structure beneath South Africa and its associated LLSVP and South African Superswell. Several hotspots are present in the Indian Ocean: La Réunion island, Kerguelen-Amsterdam, Crozet, Marion, and Comoros, and their origin at depth can be investigated. An intriguing feature resulting from SEMINDO is the existence of low-velocity conduits (Figure 11, right panel) in the depth range around 1,200 km, connecting deep large-scale (blobby) low-velocity anomalies of SEMUCB-WM1 in the lower mantle to the upper mantle transition zone (Figure 11, right panel). We observe these conduits in several cross-sections from the Southeast Indian Ridge to the Northwest, and from the Southwest Indian Ridge to the North (Figures 11e and 11f). One can also notice the presence of these conduits in other directions, from the South Africa to the Eastern part of the Indian Ocean and from the South Africa to the Northeast (Figures 11g and 11h). These observations may suggest the presence of several small-scale conduits around the Réunion hotspot, and several mantle upwellings connecting the South African LLVP to the surface hotspots, as recently evidenced by body-wave tomography by (Tsekhmistrenko et al., 2018).

The conduits appear to be broad in the upper mantle with a narrow tail in the lower mantle, anchored to the Large Low-Shear Velocity (above the CMB) from the background model. The small size of the conduit in the lower mantle may either be due to the fact that the conduit was initially much wider but emptied with time, or may reflect a very strong viscosity contrast with the surrounding lower mantle. Some cross-sections exhibit conduits which seem to be vertical (Figures 13a and 11e) and other seem to be tilted (Figures 11e and 11h). This depends on viewing angles, or may also be related to the azimuthal coverage.

Interestingly, the conduit beneath the Réunion (Figure 13a) is similar to the one found beneath Pitcairn Island in the South Pacific (in the sense that both are originating from the CMB), see Figure 1c in S. W. French & Romanowicz (2015). As for the other Indian Ocean hotspots, Marion, Kerguelen-Amsterdam, Comoros, low-velocity anomalies are observed in the upper mantle and even down to 1200 km depth for Kerguelen-Amsterdam, but we cannot dismiss the connection with the south African dome since their morphology looks more complicated, whereas the conduit beneath the Réunion hotspot is better resolved, more vertical and therefore simpler to characterize. The spread of the low-velocity anomaly observed in the upper mantle (Figure 12) may be due to the deflection of the plume conduit by the convection currents in the upper mantle (where the viscosity is at least 30 times lower than the viscosity in the lower mantle).

### 6.5. Remnant Slabs in the Transition Zone?

If the Oman and Zagros ophiolite (e.g., Lees, 1928) and belts (e.g., Reinhardt, 1968) are accepted to result from the Arabian-Eurasian collision and to the closure of the Thetys Ocean, other ophiolite belts in the North-West Indian Ocean have been proposed to be formed along Indian-Arabian/African plate boundary, resulting from a former subduction zone between India and Africa. The north-dipping fast velocity anomaly extending between the northern Triple Junction (around the Aden-Owen-Carlsberg), the Marie Celeste Fracture Zone (indicated on Figure 1b as MC-FZ) and the northern part of SEIR (Southeast Indian Ridge), passing through the CIR (Figure 8, right panel) may be the signature of the remnant Carlsberg slab entrained in the oblique subduction of Indian lithosphere beneath the Arabian/African oceanic lithosphere, as proposed by (Gaina et al., 2015). These fast velocity anomalies visible in SEMINDO are located at the position of the northern boundary of India during the Jurassic (~170 Ma); for example, Figure 9a from Gaina et al. (2015) & Figure 22b from Pearce et al. (1981), as well as that of the anomalies inferred from the reconstruction of the subducted Tethyan lithosphere (e.g., Hafkenscheid et al., 2006). They may represent remnant slabs, presently in the transition zone and the lower mantle, originating from the northward subduction of the Indian plate below the Neotethyan lithosphere.

## 7. Conclusions

We have presented a multi-mode regional tomographic model (SEMINDO) of the mantle beneath the Indian Ocean down to ~1200 km depth obtained by full waveform inversion of three component fundamental and overtone surface waves. In the upper mantle, we successfully resolve two large-scale, low-velocity anomalies on either side of the Central Indian Ridge that likely represent hot material probably issued from the lower mantle and trapped in the asthenosphere underneath the Mascarene Basin (MBAR anomaly) and the Central Indian Basin (CIOBA anomaly). The low-velocity anomaly beneath the Central Indian Ocean (CIOBA) extends down to the transition zone, whereas the MBAR anomaly located beneath the Mascarene Basin has a significant signature only down to the top of the upper transition zone at ~250 km depth. Our model evidences a connection between MBAR, Comoros and East-Africa hotspots in the uppermost mantle, which disappear at depth  $\geq 300$  km. This suggests the presence of large-scale horizontal flow between East-Africa and Réunion, and material transfer eastward to the CIR. Radial anisotropy with  $\delta\epsilon^r < 0$  is locally present around hotspots and may indicate upwelling of hot material. Our approach allows us to resolve a narrow conduit that connects low-velocities in the lower mantle to the Réunion hotspot at the earth's surface. The conduit is thin in the uppermost lower mantle ( $\leq 1200$  km), then broadens in the transition zone and finally spreads in the upper mantle beneath the Réunion hotspot and feeds the Mascarene Basin asthenosphere by horizontal flow. The remnant slab due the subduction of the Indian below the Neotethyan lithosphere during the northward Indian drift is well resolved. This regional study resolves mantle structure down to the lower mantle ~1200 km, well beyond the previous tomographic models based on fundamental mode surface wave dispersion and restricted to ~300 km depth. Our regional tomographic model of the

Indian Ocean reveals a complex mantle plume beneath the Réunion and its likely connection with the South Africa LLSVP. These findings may guide further geochemistry and geodynamic studies in the Indian Ocean to investigate potential genetic connection between Réunion and Comores volcanism. The inversion of azimuthal anisotropy in the upper and lower transition zone will be an efficient way to shed some light on the deep mantle dynamics in this region. The maximum depth sampled by higher modes being ~1200 km, the incorporation of a body waveform data set extending to shorter periods should improve the model resolution down to the CMB, and provide additional constraints on the shape of the low velocity conduit across the whole lower mantle.

## Data Availability Statement

The RHUM-RUM data set (<https://doi.org/10.15778/RESIF.YV2011>) has been assigned the FDSN network code YV and is hosted and served by the French RESIF data center (<http://seismology.resif.fr>). The additional data from Federation of Digital Seismograph Networks (FDSN) are available through (Mauria et al., 2016). We also used data from the permanent networks: GEOSCOPE <https://doi.org/10.18715/GEOSCOPE.G>, GSN: <https://doi.org/10.7914/SN/IU>, and seismic data from the temporary experiments, RHUM-RUM data <https://doi.org/10.15778/RESIF.YV2011>, Selasoma: Network <http://doi.org/10.14470/MR7567431421>, SEMINDO model is available at <https://github.com/wamba/SEMINDO>.

## Acknowledgments

This project was funded by INSPIRE (INTERdisciplinary and excellence for doctoral training of International REsearchers in Paris), Collège de France and IUF (Institut Universitaire de France), we are very thankful for that. The authors thank Haydar Karaoglu, Hugo Jiménez, Eric Debayle, Frederik J. Simons, Yann Capdeville, Jérôme Dymont, Eléonore Stutzmann and Federico Daniel Munch for their valuable discussions. Computational resources were provided by S-CAPAD (Service de calcul parallèle et de traitement de données en sciences de la Terre) & CINES (Center Informatique National de l'Enseignement Supérieur) and the authors appreciate their willingness to help. The RHUM-RUM project (<http://www.rhum-rum.net>) was funded by ANR (Agence Nationale de la Recherche) in France (project ANR-11-BS56-0013), and by DFG (Deutsche Forschungsgemeinschaft) in Germany (grants SI1538/2-1 and SI1538/4-1). We acknowledge Mike Ritzwoller and Nikolai Shapiro who readily provided their excellent group velocity data set. Many thanks to all scientists, engineers and technicians who operate permanent (FDSN networks) and temporary networks and pools of land and ocean bottom seismic stations (DEPAS, INSU, MACOMO, Gipp, RESIF-SISMOB) and data centers who made all seismic data freely available.

## References

- ASL/USGS, A. S. L. (1988). Global seismograph network (gsn-iris/usgs). International Federation of Digital Seismograph Networks.
- Backus, G. E. (1962). Long-wave elastic anisotropy produced by horizontal layering. *Journal of Geophysical Research*, 67(11), 4427–4440. <https://doi.org/10.1029/jz067i011p04427>
- Barruol, G., & Sigloch, K. (2011). Rhum-rum group. RHUM-RUM experiment 2015.
- Barruol, G., & Sigloch, K. (2013). Investigating la réunion hot spot from crust to core. *Eos, Transactions American Geophysical Union*, 94(23), 205–207. <https://doi.org/10.1002/2013eo230002>
- Barruol, G., Sigloch, K., Scholz, J.-R., Mazzullo, A., Stutzmann, E., Montagner, J.-P., et al., (2019). Large-scale flow of Indian ocean asthenosphere driven by réunion plume. *Nature Geoscience*, 12, 1–7. <https://doi.org/10.1038/s41561-019-0479-3>
- Bergman, E. A., & Solomon, S. C. (1985). Earthquake source mechanisms from body-waveform inversion and intraplate tectonics in the northern Indian ocean. *Physics of the Earth and Planetary Interiors*, 40(1), 1–23. [https://doi.org/10.1016/0031-9201\(85\)90002-0](https://doi.org/10.1016/0031-9201(85)90002-0)
- Capdeville, Y., & Marigo, J.-J. (2007). Second order homogenization of the elastic wave equation for non-periodic layered media. *Geophysical Journal International*, 170(2), 823–838. <https://doi.org/10.1111/j.1365-246x.2007.03462.x>
- Centre, G. D. (1993). *Geofon seismic network*. deutsches geoforschungszentrum gzf. Other/Seismic Network.
- Cesca, S., Letort, J., Razafindrakoto, H. N., Heimann, S., Rivalta, E., Isken, M. P., et al., (2020). Drainage of a deep magma reservoir near Mayotte inferred from seismicity and deformation. *Nature Geoscience*, 13(1), 87–93. <https://doi.org/10.1038/s41561-019-0505-5>
- Coudurier-Curveur, A., Karakaş, Ç., Singh, S., Tapponnier, P., Carton, H., & Hananto, N. (2020). Is there a nascent plate boundary in the northern Indian ocean? *Geophysical Research Letters*, 47(7), e2020GL087362. <https://doi.org/10.1029/2020GL087362>
- Courtillot, V., Davaille, A., Besse, J., & Stock, J. (2003). Three distinct types of hotspots in the earth's mantle. *Earth and Planetary Science Letters*, 205(3–4), 295–308. [https://doi.org/10.1016/s0012-821x\(02\)01048-8](https://doi.org/10.1016/s0012-821x(02)01048-8)
- Courtillot, V., Feraud, G., Maluski, H., Vandamme, D., Moreau, M., & Besse, J. (1988). Deccan flood basalts and the cretaceous/tertiary boundary. *Nature*, 333(6176), 843–846. <https://doi.org/10.1038/333843a0>
- Cupillard, P., Delavaud, E., Burgos, G., Festa, G., Vilotte, J.-P., Capdeville, Y., & Montagner, J.-P. (2012). Regsem: A versatile code based on the spectral element method to compute seismic wave propagation at the regional scale. *Geophysical Journal International*, 188(3), 1203–1220. <https://doi.org/10.1111/j.1365-246x.2011.05311.x>
- Davaille, A., Stutzmann, E., Silveira, G., Besse, J., & Courtillot, V. (2005). Convective patterns under the indo-Atlantic box. *Earth and Planetary Science Letters*, 239(3–4), 233–252. <https://doi.org/10.1016/j.epsl.2005.07.024>
- Debayle, E., & Lévêque, J. (1997). Upper mantle heterogeneities in the Indian Ocean from waveform inversion. *Geophysical Research Letters*, 24(3), 245–248. <https://doi.org/10.1029/96gl03954>
- Debayle, E., & Ricard, Y. (2012). A global shear velocity model of the upper mantle from fundamental and higher rayleigh mode measurements. *Journal of Geophysical Research*, 117(B10), B10308. <https://doi.org/10.1029/2012jb009288>
- Duncan, R. A., Backman, J., & Peterson, L. C. (1990). The volcanic record of the reunion hotspot. In Proceedings of the Ocean Drilling Program Scientific Results. (Vol. 115, pp. 3–10).
- Festa, G., & Vilotte, J.-P. (2005). The newmark scheme as velocity–stress time-staggering: An efficient pml implementation for spectral element simulations of elastodynamics. *Geophysical Journal International*, 161(3), 789–812. <https://doi.org/10.1111/j.1365-246x.2005.02601.x>
- Forte, A. M., Quéré, S., Moucha, R., Simmons, N. A., Grand, S. P., Mitrovica, J. X., & Rowley, D. B. (2010). Joint seismic–geodynamic–mineral physical modeling of african geodynamics: A reconciliation of deep-mantle convection with surface geophysical constraints. *Earth and Planetary Science Letters*, 295(3–4), 329–341. <https://doi.org/10.1016/j.epsl.2010.03.017>
- French, S., Lekic, V., & Romanowicz, B. (2013). Waveform tomography reveals channeled flow at the base of the oceanic asthenosphere. *Science*, 342(6155), 227–230. <https://doi.org/10.1126/science.1241514>
- French, S. W., & Romanowicz, B. (2014). Whole-mantle radially anisotropic shear velocity structure from spectral-element waveform tomography. *Geophysical Journal International*, 199(3), 1303–1327. <https://doi.org/10.1093/gji/ggu334>
- French, S. W., & Romanowicz, B. (2015). Broad plumes rooted at the base of the earth's mantle beneath major hotspots. *Nature*, 525(7567), 95–99. <https://doi.org/10.1038/nature14876>



- Gaina, C., Van Hinsbergen, D. J., & Spakman, W. (2015). Tectonic interactions between India and Arabia since the Jurassic reconstructed from marine geophysics, ophiolite geology, and seismic tomography. *Tectonics*, 34(5), 875–906. <https://doi.org/10.1002/2014tc003780>
- GEOSCOPE (1982). *French global network of broad band seismic stations*. Institut de Physique du Globe de Paris & Ecole et Observatoire des Sciences.
- Hable, S., Sigloch, K., Stutzmann, E., Kiselev, S., & Barruol, G. (2019). Tomography of crust and lithosphere in the western Indian ocean from noise cross-correlations of land and ocean bottom seismometers. *Geophysical Journal International*, 219(2), 924–944. <https://doi.org/10.1093/gji/ggz333>
- Hafkenscheid, E., Wortel, M., & Spakman, W. (2006). Subduction history of the tethyan region derived from seismic tomography and tectonic reconstructions. *Journal of Geophysical Research*, 111(B8), B08401. <https://doi.org/10.1029/2005jb003791>
- Iaffaldano, G., Davies, D., & DeMets, C. (2018). Indian Ocean floor deformation induced by the reunion plume rather than the Tibetan plateau. *Nature Geoscience*, 11(5), 362–366. <https://doi.org/10.1038/s41561-018-0110-z>
- Institute Of Geophysics China Earthquake Administration (IGPCEA). (2007). *Data management centre of china national seismic network at institute of geophysics, cea*. Data Management Centre of China National Seismic Network at Institute of Geophysics, CEA. <https://doi.org/10.7914/SN/CB>
- Komatitsch, D., & Tromp, J. (1999). Introduction to the spectral element method for three-dimensional seismic wave propagation. *Geophysical Journal International*, 139(3), 806–822. <https://doi.org/10.1046/j.1365-246x.1999.00967.x>
- Kustowski, B., Ekström, G., & Dziewoński, A. (2008). Anisotropic shear-wave velocity structure of the earth's mantle: A global model. *Journal of Geophysical Research*, 113(B6), B06306. <https://doi.org/10.1029/2007jb005169>
- Lees, G. M. (1928). The geology and tectonics of oman and of parts of south-eastern Arabia. *Quarterly Journal of the Geological Society*, 84(1–4), 585–670. <https://doi.org/10.1144/gsl.jgs.1928.084.01-04.24>
- Lekić, V., & Romanowicz, B. (2011). Inferring upper-mantle structure by full waveform tomography with the spectral element method. *Geophysical Journal International*, 185(2), 799–831.
- Lévesque, J., Debayle, E., & Maupin, V. (1998). Anisotropy in the Indian ocean upper mantle from rayleigh-and love-waveform inversion. *Geophysical Journal International*, 133(3), 529–540. <https://doi.org/10.1046/j.1365-246x.1998.00504.x>
- Li, X.-D., & Romanowicz, B. (1995). Comparison of global waveform inversions with and without considering cross-branch modal coupling. *Geophysical Journal International*, 121(3), 695–709. <https://doi.org/10.1111/j.1365-246x.1995.tb06432.x>
- Li, X.-D., & Romanowicz, B. (1996). Global mantle shear velocity model developed using nonlinear asymptotic coupling theory. *Journal of Geophysical Research*, 101(B10), 22245–22272. <https://doi.org/10.1029/96jb01306>
- Love, A (1927). *A treatise on the mathematical theory of elasticity*. Dover publ.
- Maurya, S., Montagner, J.-P., Kumar, M. R., Stutzmann, E., Kiselev, S., Burgos, G., et al. (2016). Imaging the lithospheric structure beneath the Indian continent. *Journal of Geophysical Research: Solid Earth*, 121(10), 7450–7468. <https://doi.org/10.1002/2016jb012948>
- Mazzullo, A., Stutzmann, E., Montagner, J.-P., Kiselev, S., Maurya, S., Barruol, G., & Sigloch, K. (2017). Anisotropic tomography around la Réunion Island from rayleigh waves. *Journal of Geophysical Research: Solid Earth*, 122(11), 9132–9148. <https://doi.org/10.1002/2017jb014354>
- Michon, L. (2016). The volcanism of the comoros archipelago integrated at a regional scale. In *Active volcanoes of the southwest Indian ocean* (pp. 333–344). Springer. [https://doi.org/10.1007/978-3-642-31395-0\\_21](https://doi.org/10.1007/978-3-642-31395-0_21)
- Montagner, J.-P. (1986). 3-dimensional structure of the Indian ocean inferred from long period surface waves. *Geophysical Research Letters*, 13(4), 315–318. <https://doi.org/10.1029/gl013i004p00315>
- Montagner, J.-P., & Anderson, D. L. (1989). Petrological constraints on seismic anisotropy. *Physics of the Earth and Planetary Interiors*, 54(1–2), 82–105. [https://doi.org/10.1016/0031-9201\(89\)90189-1](https://doi.org/10.1016/0031-9201(89)90189-1)
- Montagner, J.-P., & Jobert, N. (1988). Vectorial tomography—II. application to the Indian ocean. *Geophysical Journal International*, 94(2), 309–344. <https://doi.org/10.1111/j.1365-246x.1988.tb05904.x>
- Montagner, J.-P., & Ritsema, J. (2001). Interactions between ridges and plumes. *Science*, 294(5546), 1472–1473. <https://doi.org/10.1126/science.1067486>
- Morgan, W. J. (1971). Convection plumes in the lower mantle. *Nature*, 230(5288), 42–43. <https://doi.org/10.1038/230042a0>
- Morgan, W. J. (1978). Rodriguez, Darwin, Amsterdam, a second type of hotspot island. *Journal of Geophysical Research*, 83(B11), 5355–5360. <https://doi.org/10.1029/jb083ib11p05355>
- Negi, J., Thakur, N., & Agrawal, P. (1987). Can depression of the core-mantle interface cause coincident Magsat and geoidal 'lows' of the central Indian ocean? *Physics of the Earth and Planetary Interiors*, 45(1), 68–74. [https://doi.org/10.1016/0031-9201\(87\)90198-1](https://doi.org/10.1016/0031-9201(87)90198-1)
- Pearce, J. A., Alabaster, T., Shelton, A., & Searle, M. P. (1981). The oman ophiolite as a cretaceous arc-basin complex: Evidence and implications. *Philosophical Transactions of the Royal Society of London - Series A: Mathematical and Physical Sciences*, 300(1454), 299–317. <https://doi.org/10.1098/rsta.1981.0066>
- Penn State University. (2004). *Africaarray. International federation of digital Seismograph networks*. Retrieved from <https://doi.org/10.7914/SN/AF>
- Reinhardt, B. (1968). On the genesis and emplacement of ophiolites in the Oman mountains geosyncline. Koninklijke/Shell exploratie en produktie laboratorium.
- RESIF. (1995). Resif-rlbp french broad-band network, resif-rap strong motion network and other seismic stations in metropolitan france. resif-réseau sismologique et géodésique français.
- Ritsema, J., Deuss, a. A., Van Heijst, H., & Woodhouse, J. (2011). S40rts: A degree-40 shear-velocity model for the mantle from new rayleigh wave dispersion, teleseismic traveltimes and normal-mode splitting function measurements. *Geophysical Journal International*, 184(3), 1223–1236. <https://doi.org/10.1111/j.1365-246x.2010.04884.x>
- Romanowicz, B. A., Panning, M. P., Gung, Y., & Capdeville, Y. (2008). On the computation of long period seismograms in a 3-d earth using normal mode based approximations. *Geophysical Journal International*, 175(2), 520–536. <https://doi.org/10.1111/j.1365-246x.2008.03914.x>
- Sauter, D., Cannat, M., Meyzen, C., Bezos, A., Patriat, P., Humler, E., & Debayle, E. (2009). Propagation of a melting anomaly along the ultraslow southwest indian ridge between 46°e and 52° 20' e: Interaction with the crozet hotspot? *Geophysical Journal International*, 179(2), 687–699. <https://doi.org/10.1111/j.1365-246x.2009.04308.x>
- Scholz, J.-R., Barruol, G., Fontaine, F. R., Mazzullo, A., Montagner, J.-P., Stutzmann, E., et al. (2018). Sks splitting in the western Indian ocean from land and seafloor seismometers: Plume, plate and ridge signatures. *Earth and Planetary Science Letters*, 498, 169–184. <https://doi.org/10.1016/j.epsl.2018.06.033>
- Scripps Institution of Oceanography. (1986). Iris/ida seismic network. In *International federation of digital Seismograph networks*. <https://doi.org/10.7914/SN/II>

- Tarantola, A. (1984). Inversion of seismic reflection data in the acoustic approximation. *Geophysics*, 49(8), 1259–1266. <https://doi.org/10.1190/1.1441754>
- Tarantola, A., & Valette, B. (1982). Generalized nonlinear inverse problems solved using the least squares criterion. *Reviews of Geophysics*, 20(2), 219–232. <https://doi.org/10.1029/rg020i002p00219>
- Tilmann, F., Yuan, X., Rumpker, G., & Rindraharisaona, E. (2012). *Selasoma project, Madagascar 2012–2014*. deutsches geoforschungszen-trum gfg. seismic network
- Torsvik, T. H., Smethurst, M. A., Burke, K., & Steinberger, B. (2006). Large igneous provinces generated from the margins of the large low-velocity provinces in the deep mantle. *Geophysical Journal International*, 167(3), 1447–1460. <https://doi.org/10.1111/j.1365-246x.2006.03158.x>
- Tsekhmistrenko, M., Sigloch, K., & Hosseini, K. (2018). *Whole-mantle structure under the reunion hotspot in the western Indian ocean from multifrequency p-wave tomography*. EGUGA. (Vol. 1076).
- van derLee, S., Regenauer-Lieb, K., & Yuen, D. A. (2008). The role of water in connecting past and future episodes of subduction. *Earth and Planetary Science Letters*, 273(1–2), 15–27. <https://doi.org/10.1016/j.epsl.2008.04.041>
- Virieux, J., & Operto, S. (2009). An overview of full-waveform inversion in exploration geophysics. *Geophysics*, 74(6), WCC1–WCC26. <https://doi.org/10.1190/1.3238367>
- Wang, Z., & Dahlen, F. (1995). Spherical-spline parameterization of three-dimensional earth models. *Geophysical Research Letters*, 22(22), 3099–3102. <https://doi.org/10.1029/95gl03080>
- Woodhouse, J. H., & Dziewonski, A. M. (1984). Mapping the upper mantle: Three-dimensional modeling of earth structure by inversion of seismic waveforms. *Journal of Geophysical Research*, 89(B7), 5953–5986. <https://doi.org/10.1029/jb089ib07p05953>
- Wysession, M., Wiens, D., & Nyblade, A. (2011). Investigation of sources of intraplate volcanism using pascall broadband instruments in madagascar, the comores, and mozambique. doi, 10. Other/Seismic Network.TUD QC